European Journal of Pharmaceutical Sciences 214 (2025) 107269

Contents lists available at ScienceDirect

European Journal of Pharmaceutical Sciences

journal homepage: www.elsevier.com/locate/ejps

# Automated 3D printing of pediatric furosemide tablets: A personalized medicine approach using semi-solid extrusion and NIR monitoring

Farnaz Shokraneh [a,b,*], Anne M. Filppula [a], Aleksi Tornio [c,d], Jaan Aruväli [e], Urve Paaver [f], Ivan Kassamakov [g], Niklas Sandler Topelius [a,b]

[a] Pharmaceutical Sciences Laboratory, Faculty of Science and Engineering, Åbo Akademi University, BioCity, Tykistökatu 6A, Turku FI-20520, Finland
[b] CurifyLabs Oy, Salmisaarenaukio 1, Helsinki FI-00180, Finland
[c] Integrative Physiology and Pharmacology, Institute of Biomedicine, University of Turku, Kiinamyllynkatu 10, Turku FI-20520, Finland
[d] Unit of Clinical Pharmacology, Turku University Hospital, Kiinamyllynkatu 10, Turku 20520, Finland
[e] Department of Geology, Institute of Ecology and Earth Sciences, University of Tartu, Ravila 14a, Tartu 50411, Estonia
[f] Faculty of Medicine, Institute of Pharmacy, Tartu University, Nooruse 1, Tartu EE-50411, Estonia
[g] Electronics Laboratory, Department of Physics, University of Helsinki, P.O. Box 64 (Gustaf Hällströmin katu 2a), FI-00014, Finland

ARTICLE INFO

*Keywords:*
3D printing
Personalized medicine
Furosemide
Near-infrared spectroscopy (NIR)
Quality control

ABSTRACT

This study presents the development of personalized, immediate-release furosemide tablets for pediatric use using semi-solid extrusion (SSE) 3D printing integrated with compounding system solution (CSS) technology. Dose personalization and real-time quality assurance were implemented using near-infrared (NIR) spectroscopy with partial least squares (PLS) modeling, supported by Fourier-transform infrared spectroscopy (FTIR), X-ray diffraction (XRD), and surface characterization via scanning white light interferometry (SWLI).

Furosemide formulations (1 % and 2 % w/w) were prepared using a gel-based excipient and printed in doses from 2 to 10 mg. The NIR-based PLS model exhibited strong predictive accuracy ($R^2 = 0.91$; RMSEC = 3.37 %), enabling effective, non-destructive blend uniformity monitoring. All formulations met European Pharmacopoeia requirements for drug content (85.0–115.0 %) and content uniformity (AV < 15). Dissolution testing confirmed rapid release profiles, with >85 % release for all freshly prepared tablets. After six months, the 2 % formulation retained adequate performance (88.5 %), while the 1 % formulation showed a moderate decline (76.3 %).

FTIR and XRD analyses revealed no significant drug–excipient interactions, and the crystalline structure of furosemide remained intact throughout storage. SWLI demonstrated surface morphology variations between formulations, revealing that excipient and surfactant levels influenced microtopography and potentially drug release kinetics.

The integration of SSE 3D printing with spectroscopic and imaging tools offers a robust, reproducible, and patient-centric platform for personalized pediatric drug manufacturing. This approach supports the transition toward automated, non-sterile compounding with real-time control, improved dose precision, and enhanced product quality—addressing long-standing gaps in pediatric pharmaceutical care.

## 1. Introduction

The convergence of 3D printing and automation technologies is revolutionizing pharmaceutical manufacturing, enabling personalized, on-demand medication production (Norman et al., 2017; Sandler and Preis, 2016). Among various additive manufacturing techniques, semi-solid extrusion (SSE) offers unique advantages for clinical pharmacy applications due to its low-temperature operation and compatibility with heat-sensitive compounds. This method allows the precise fabrication of customized solid oral dosage forms, making it particularly suitable for pediatric pharmacotherapy, where age-appropriate formulations and individualized dosing are critically needed (Alhnan et al., 2016; Goyanes et al., 2017).

Advances in automated manufacturing methods, such as SSE, are enhancing the precision, scalability, and personalization of customized dosage forms. Incorporating online quality control systems can further strengthen reliability and consistency, supporting the broader clinical adoption of individualized therapies. Conventional quality control (QC)

* Corresponding author at: Åbo Akademi University, BioCity, Tykistökatu 6A, Turku FI-20520, Finland
*E-mail addresses:* Farnaz.shokraneh@abo.fi, Farnaz.shokraneh@curifylabs.com (F. Shokraneh).

https://doi.org/10.1016/j.ejps.2025.107269
Received 18 June 2025; Received in revised form 6 September 2025; Accepted 9 September 2025
Available online 10 September 2025

tools such as high-performance liquid chromatography (HPLC), dissolution, or disintegration testing are destructive, resource-intensive, and unsuitable for point-of-care compounding (Khaled et al., 2014; Yu and Ding, 2008). In contrast, Near-Infrared (NIR) spectroscopy, when applied with chemometric modeling, has emerged as a non-destructive Process Analytical Technology (PAT) for pharmaceutical manufacturing (Blanco and Villarroya, 2002; Roggo et al., 2007). It enables real-time monitoring of blend uniformity (BU) and active pharmaceutical ingredient (API) content, offering immediate feedback on formulation quality before and during the printing process (De Beer et al., 2011; Markl and Zeitler, 2017).

One drug that highlights the urgent need for personalised precision dosing is furosemide, a loop diuretic frequently prescribed to manage fluid overload in children, particularly those undergoing cardiac surgery or living with heart failure (Prandota, 2001a; van der Vorst et al., 2006). Pediatric dosing typically ranges from 1 to 2 mg/kg for patients with normal renal function. However, due to a prolonged elimination half-life in infants, furosemide is associated with risks of drug accumulation, potentially leading to sensorineural hearing loss, hypovolemia, gallstones, and electrolyte imbalances (Whitelaw et al., 2001). Despite these clinical challenges, there are no approved pediatric-specific solid dosage forms, and compounded alternatives often suffer from inconsistent dosing accuracy, instability, and poor microbiological quality (Eileen Kairuz et al., 2007; Van Der Zanden et al., 2021; Van Riet-Nales et al., 2011).

Previous research has explored the feasibility of 3D printed furosemide formulations, e.g. Lafeber et al. (2021) who produced 3D-printed furosemide and sildenafil tablets. While the work highlighted the innovative potential of 3D printing and addressed aspects of dose accuracy and content uniformity, it did not implement real-time process control, nor did it conduct a complete pharmacopeial QC assessment or long-term stability testing. Similarly, other SSE-based approaches have focused on proof-of-concept fabrication and basic characterization, without addressing multi-stage quality assurance, blend homogeneity, or microbial stability (Awad et al., 2018; Trenfield et al., 2018).

Despite these technological advancements, the practical integration of 3D printing and semi-solid extrusion into hospital and compounding pharmacy settings remains limited (Gudeman et al., 2013; Rinke et al., 2007). Challenges include equipment complexity, the need for specialized operator training, the absence of standardized operating procedures, and concerns about maintaining pharmacopeial quality standards outside traditional manufacturing environments (Johannesson et al., 2023). Furthermore, the lack of integrated, real-time quality assurance measures often undermines confidence in the reliability and reproducibility of individualized dosage forms (Mullarkey, 2009). Addressing these gaps is essential to support the broader clinical adoption of on-demand personalized medicine, particularly for vulnerable patient groups such as children.

This study presents a scalable approach to personalized pediatric furosemide tablets using SSE-based 3D printing and compounding system technology. It integrates NIR spectroscopy and chemometric analysis for real-time blend monitoring, along with on-line mass uniformity testing. Quality control aligns with European Pharmacopoeia (Ph. Eur). Standards (The European Pharmacopoeia. Version 11.0), January 2023), covering content uniformity, pharmacopeial tests, and a six-month stability study. The work establishes a comprehensive framework for in-process and post-process quality assurance in automated, pharmacy-based manufacturing of personalized medicines.

## 2. Materials and methods

### 2.1. Materials

Furosemide secondary standard was obtained from Merck (New Jersey, USA), while the Ph. Eur. grade API and polysorbate 80 were sourced from Caesar & Loretz GmbH (Hilden, Germany). CuraBlend® gel tablet excipient base from CurifyLabs Oy (Helsinki, Finland), was used for preparing extrudable mixtures. CuraBlend® is composed of purified water, xylitol, gelatin, cocoa butter, glycerol, maltodextrin, citric acid, sodium citrate, potassium sorbate, and flavors. All solvents and reagents used were of analytical grade.

Tablets were packaged in Mini Medi-Cup® Plus™ Blisters (MD425) from Medi-Dose Group (Pennsylvania, USA) and sealed using Laser-Label™ "25″ Lid-Label® cover sheets from the same supplier.

### 2.2. Methods

#### 2.2.1. The modelling methodology for NIR/PLS development

*2.2.1.1. Preparation of calibration samples.* Calibration samples were prepared for blend uniformity (BU) testing using an excipient base. Initially, separate 10 % w/w stock formulations of furosemide API were created. These stock formulations included the API along with polysorbate and excipient base as an excipient base. For furosemide stock formulation, a 1 % polysorbate 80 concentration was used. Each stock formulation was diluted with excipient base to achieve concentrations ranging from 80 % to 120 % w/w. For each drug, the appropriate polysorbate 80 concentration was mixed with the respective API before blending with excipient base using a PM140 mixer, supplied by Gako Deutschland GmbH (Scheßlitz, Germany) for 10 min per batch. Following this, multiple external validation batches were prepared for both drugs using the same methodology. In the second phase of the study, to enhance sampling techniques, the same sample preparation process was repeated three times, with each set containing nine concentrations within the range of 80.0 % to 120.0 %.

*2.2.1.2. Spectral acquisition.* The collection of spectra for at-line samples was conducted using the VIAVI micro NIR spectrophotometer (California, USA). This MicroNIR employs a linear variable filter as its dispersing element — a band-pass filter with a linearly varying transmitted wavelength across its surface. Coupled to an uncooled 128-pixel InGaAs linear diode array, each pixel of the array detects and reads out a different wavelength. The light source consists of a pair of low-power vacuum tungsten lamps, and a 16-bit analog-to-digital converter is utilized for sample data digitization.

The spectrophotometer operates within a spectral range of 980–1800 in reflectance mode at 0.1 ms intervals, with a 100-scan count. It boasts a wavelength accuracy of $<1$ nm and wavelength reproducibility of $<0.1$ nm.

MicroNIR droplet sampler, supplied by VIAVI (California, USA), was utilized for the analysis of blend uniformity in the CuraBlend matrix. Key specifications of the MicroNIR Droplet Sampler include a 250 μm dual-pass cell, resulting in a total path length of 500 μm. This configuration allows for accurate spectral analysis with only a few drops of the sample. Additionally, the accessory is equipped with a built-in diffuse reflectance reference, ensuring consistent and reproducible measurements. Fig. 1 illustrates the sample preparation process for NIR spectroscopic analysis.

*2.2.1.3. Chemometric spectral data treatment.* Spectral preprocessing and multivariate analysis were conducted utilizing the chemometric software VIAVI MicroNIR TM Pro Version 3.2 (California, USA). Preprocessing techniques employed included standard normal variate (SNV) correction and first derivative with smoothing (Rinnan et al., 2009). These methods were used to amplify the chemical characteristic signals of the blends while minimizing noise associated with their physical properties.

*2.2.1.4. Calibration model development.* The calibration models were evaluated using criteria such as root mean square error of calibration (RMSEC), root mean square error of cross-validation (RMSECV) using


**Fig. 1.** Sample preparation for near-infrared (NIR) spectroscopic analysis using drop-on-window technique:
Step 1: A small amount of semi-solid formulation is dispensed onto the measurement window of the NIR sample holder using a syringe.
Step 2: The holder is closed to ensure uniform sample spreading across the window.
Step 3: The sample is inserted into the NIR spectrometer for spectral data acquisition.
This method enables non-destructive, contact-free analysis of semi-solid materials.

the leave-one-out technique, and the number of latent variables (LV). Analysis of these parameters in pre-processing determined the optimal model. Preference was given to the model with the lowest RMSECV values and the fewest LVs. Additionally, the performance of the established model was assessed using an external validation set of samples, comparing discrepancies with a reference method to demonstrate the efficacy of the developed partial least squares (PLS) models for both spectroscopic methods (De Bleye et al., 2012).

*2.2.1.5. NIR method validation.* The validated final PLS models for BU were updated in accordance with NIR method guidelines (Development and Submission of Near Infrared Analytical Procedures, 2021). The validation process encompassed assessments for accuracy, linearity, precision and robustness using external validation samples independent of the calibration samples. To assess accuracy, the NIR model's predictions for offline BU monitoring were compared to the mean HPLC data of blends extracted from 10 locations of the 3D printer syringe. Accuracy was statistically determined by evaluating the closeness of NIR

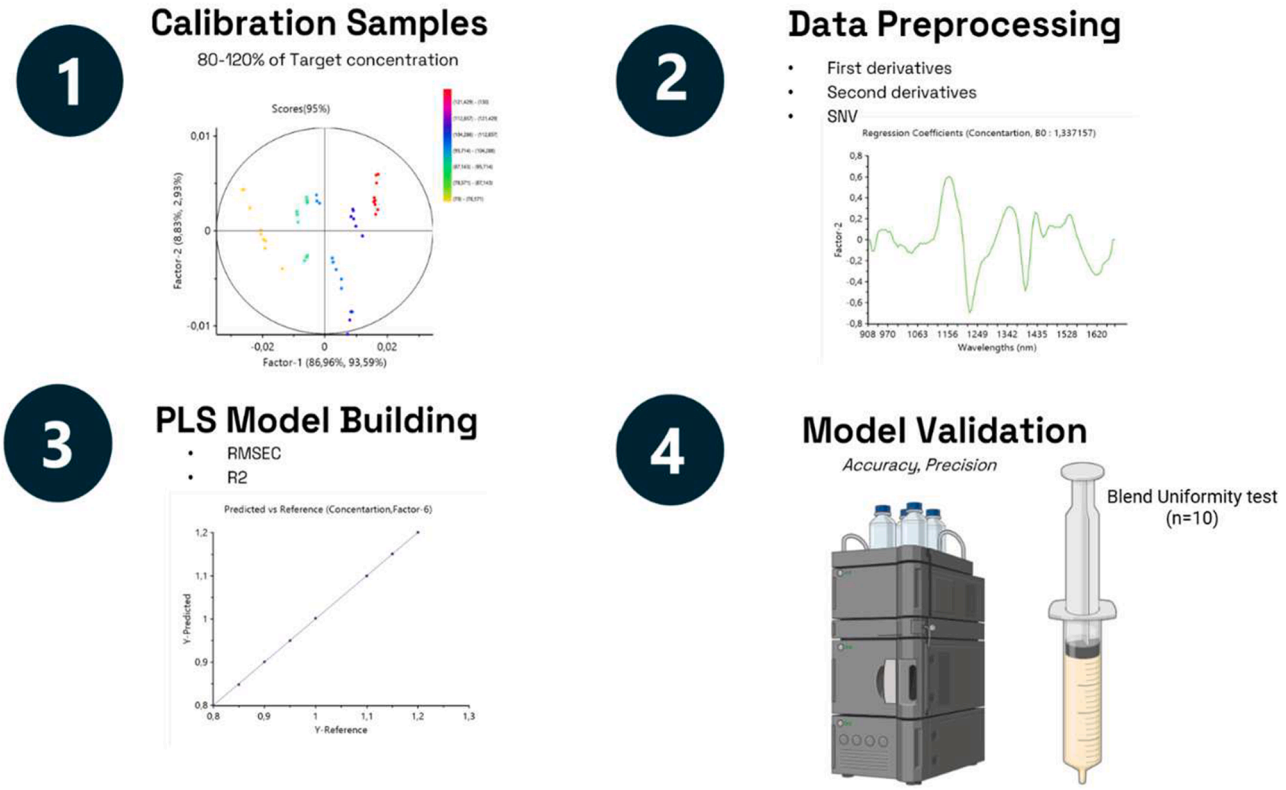


**Fig. 2.** Workflow for developing and validating a PLS model for BU analysis:
(1) *Calibration*: Samples spanning 80–120 % of the target concentration ensured representative data coverage, confirmed by multivariate score plots. (2) *Preprocessing*: Spectra were treated with derivative and standard normal variate (SNV) corrections; regression plots identified key predictive regions. (3) *Model Building*: Spectral data were correlated with reference values; performance assessed via root mean square error of calibration (RMSEC), coefficient of determination ($R^2$), and prediction accuracy (4) *Validation*: The model's accuracy and precision were validated in a real-world belnd uniformity setup.

BU data to the target 100 %.

A precision test as a repeatability was conducted by measuring one sample at different concentration levels: 80 %, 100 %, and 110 %. Each concentration level was tested, and measurements were taken 6 times for each 10 samples. Relative standard deviation (RSD %) was calculated for each set of 6 measurements, and the average RSD % for each sample level and factor combination was computed. Linearity was established within the range of 80–110 % of the target API concentration for the BU method. Robustness testing involved executing batches with different API concentrations (ranging from 80 % to 110 % for BU) and varied batch sizes of formulations (50 g, 60 g and 70 g) (Fig. 2).

A detailed NIR-based chemometric approach was employed for BU assessment. Calibration samples were prepared across a concentration range (80–120 %) using an excipient base. Spectral acquisition was performed using a MicroNIR spectrophotometer with a drop-on-window technique, enabling non-destructive sampling. Chemometric treatment and model development were conducted using standard preprocessing and Partial Least Squares (PLS) regression analysis. The final models were validated in accordance with FDA guidance, including evaluations for accuracy, precision, linearity, and robustness.

### 2.2.2. Pre formulation studies assessing drug-excipient interactions

*2.2.2.1. Fourier-transform infrared spectroscopy.* Fourier-transform infrared spectroscopy (FTIR) spectra of the raw materials and extruded gel tablets were acquired using a Shimadzu IRPrestige-21 spectrophotometer (Kyoto, Japan), fitted with a Golden Gate ATR accessory from Specac Ltd. (Orpington, UK). Measurements were performed at three distinct points on each tablet surface. Individual spectra of all solid components were also taken one by one.

*2.2.2.2. X-ray powder diffraction.* X-ray Powder Diffraction (XRPD) patterns of furosemide raw materials and extruded gel-based tablets were recorded using a D8 Advance X-ray diffractometer (Bruker AXS GmbH, Karlsruhe, Germany). Measurements were performed in symmetrical reflection mode using Bragg-Brentano geometry, with CuKα radiation ($\lambda = 1.54$ Å). Data were collected over a 2θ range of 5° to 35°, with a step size of 0.2° 2θ. Scattered X-ray intensities were detected using a LynxEye one-dimensional detector equipped with 165 channels. The instrument was operated at 40 kV and 40 mA. XRPD analysis was conducted on the semi-solid CuraBlend® base as well as the physical mixture of all solid components, and individual solid ingredients from the formulation, such as cocoa butter, xylitol and furosemide. Each tablet was measured individually immediately after removal from the blister pack to minimize drying of the tablets during measurement.

### 2.2.3. The formulation process including SSE printing and compounding steps

*2.2.3.1. Formulation of furosemide tablets.* A formulation with 1 % furosemide was prepared using CuraBlend® as the base (98.0 % w/w), with polysorbate 80 and furosemide each contributing 1 % w/w. In comparison, a 2 % furosemide formulation comprised 96.0 % w/w excipient base, along with 2 % w/w of both polysorbate 80 and furosemide. Homogenization of each formulation was performed using an automated planetary mixing unit (PM 140, Gako Deutschland GmbH, Scheblitz, Germany) set to 2800 rpm for a duration of 10 min. After mixing, the molten blends were aseptically loaded into pre-sterilized, disposable 100 mL polyvinyl chloride (PVC) syringes fitted with Luer-lock connectors (CurifyLabs, Helsinki, Finland).

To accommodate varying dosage requirements, tablets were produced in multiple sizes corresponding to different drug strengths. Specifically, for the 1 % furosemide formulation, tablets containing 1, 2, 3, 4, and 5 mg of the active ingredient were manufactured, while the 2 % formulation yielded tablets with 2, 4, 6, 8, and 10 mg of furosemide, thereby enabling a flexible range of therapeutic dosing options.

*2.2.3.2. Integrated compounding platform.* The compounding workflow in this study was implemented using CurifyLabs' Compounding System Solution (CSS, CurifyLabs, Helsinki, Finland), a semi-automated platform (Fig. 3) designed for non-sterile pharmaceutical manufacturing, which integrates digital formulation management, planetary mixing, and semi-solid extrusion (SSE) 3D printing for the preparation of individualized solid oral dosage forms. (Sandler Topelius et al., 2024).

*2.2.3.3. In-process homogeneity study of syringe-loaded formulation.* A 100 g batch was loaded into a 100 mL syringe and printed using a 3D Pharma Printer set at 40 °C. To evaluate the uniformity of the material dispensed throughout the printing cycle, samples were collected at three distinct stages. At the start of the process, three units were taken from the first, third, and last rows of the blister pack. The same sampling pattern was repeated at the midpoint of printing. At the end, four units were collected—three from the defined rows and one randomly selected. This structured sampling approach allowed for a cross-sectional assessment of content consistency throughout the entire run, ensuring material homogeneity within the syringe.

### 2.2.4. Tablet characterization methods

*2.2.4.1. HPLC-based assay for furosemide content.* Furosemide quantification was carried out using a validated HPLC method in line with ICH Guideline Q2. The analysis utilized an HPLC system from Waters Corporation (Milford, Massachusetts, USA) equipped with a photodiode array (PDA) detector. Chromatographic separation was performed on a BEH C18 VanGuard FIT column (2.5 μm, 100 mm), operated at ambient temperature. The mobile phase was composed of 10 mM potassium phosphate monobasic (prepared by dissolving 1.2 g in 1000 mL of water) and acetonitrile in a 70:30 ratio. The pH was adjusted to 3.5 using phosphoric acid. The method employed a flow rate of 1 mL/min, a detection wavelength of 233 nm, an injection volume of 5 μL, and a total analysis time of 8.0 min. To create analytical stock reference standard solutions, 50 mg of furosemide was dissolved in 500.0 mL of a diluent composed of a 50:50 vol-to-volume ratio (v/v) mixture of methanol and water. 5.0 mL of the solution was further diluted to 10.0 mL with diluent. For sample preparation, furosemide tablet samples of various doses were prepared to achieve a concentration of 50 ppm.

The quantification of furosemide content in tablets was performed using Waters Empower software (version 3.6.1). To prepare assay samples at a target concentration of 50 ppm, 500 mg of a tablet formulation containing 1 % furosemide was dissolved in 50 mL of the mobile phase. The solution was then heated in a water bath at 50 °C, vortexed to ensure complete dissolution, and subsequently filtered using a 0.2 μm membrane filter. This process yielded a final sample concentration of 50 ppm.

To evaluate dosage uniformity within each batch, content analysis was conducted on 10 individual tablets. The results were assessed in accordance with the Ph. Eur. standard 2.9.40, which outlines the criteria for content uniformity of dosage units.

The content uniformity was expressed through the Acceptance Value (AV), as described in Ph. Eur. chapter 2.9.40, which is calculated using both the mean content of the tested units and the variability among them. This approach ensures that each unit within the batch falls within acceptable limits defined in the respective monograph.

*2.2.4.2. Disintegration time.* The disintegration behavior of furosemide tablets was examined using a DT2 disintegration tester (Sotax, Allschwil, Switzerland), in alignment with the Ph. Eur. section 2.9.1, which sets a 15-minute maximum limit for uncoated tablets. The evaluation took place in 1-liter beakers containing purified water held at a temperature of 37 °C. Six individual tablets, each with a mass of 400 mg, were tested

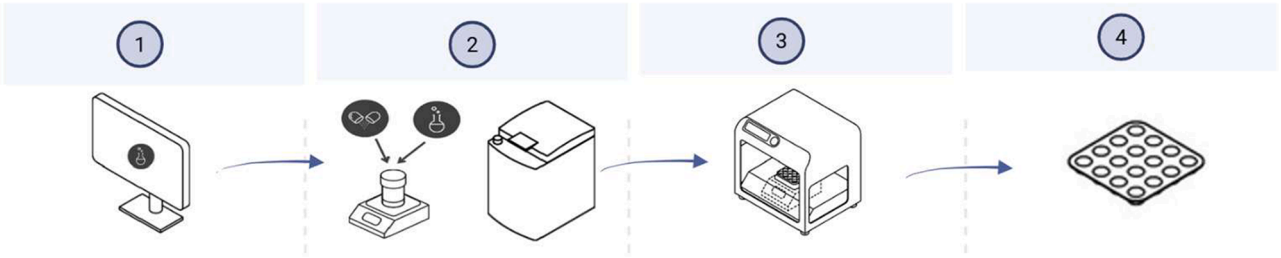


**Fig. 3.** Workflow for compounding platform.
*Step 1*: Batch preparation and order creation: batch protocols are retrieved from the validated formulation library.
*Step 2*: Ingredient addition and homogeneous mixing: The active pharmaceutical ingredient (API) powder and Polysorbate 80 (PS80) are combined with the CuraBlend® excipient base. Ingredients are mixed using an automated high-speed mixer according to the defined batch protocol.
*Step 3*: 3D printing and in-process quality control: Customized tablets are manufactured directly into blister moulds using a precision 3D printing unit. Each tablet undergoes 100 % in-process mass verification to ensure compliance with dosage and weight specifications. *Step 4*: Blister sealing and product release: completed tablets are sealed into labelled blisters and released following final quality control analysis.

($n = 6$). The time taken for each tablet to fully disintegrate was recorded, marking the point at which no solid residue remained.

*2.2.4.3. In vitro drug release measurements.* Purified water served as the dissolution medium for testing. For tablets containing 400 mg of furosemide, the test volume was fixed at 500 mL, and the temperature was kept steady at 37 °C throughout the procedure. The analysis was carried out using a Waters Acquity 2998 photodiode array HPLC system (Milford, Massachusetts, USA), in conjunction with a dissolution apparatus equipped with paddles (ERWEKA GmbH, Langen, Germany). Tablet dissolution was monitored at predefined intervals: 0, 5, 10, 15, 20, 30, 45, and 60 min, with the paddle speed consistently maintained at 50 rpm. Each test involved six tablets of the same dosage strength.

The dissolution testing followed the specifications outlined in the Ph. Eur. sections 2.9.3 (Table 1) and 5.17.1, which pertain to standard immediate-release solid oral dosage forms. Analytical evaluation was performed based on the method detailed in section 2.5. According to the defined acceptance criteria, a minimum of 80 % (Q) of the declared furosemide content must dissolve within 60 min during the first stage of testing with six units.

*2.2.4.4. pH determination.* The pH evaluation of the furosemide tablets was conducted at ambient temperature using an Edge pH meter (HANNA Instruments Inc., Woonsocket, USA). For this assessment, three tablets, each containing 400 mg of furosemide ($n = 3$), were placed in individual glass containers and gently heated to 45 °C to allow softening. After approximately 30 s, the pH probe was introduced into the liquefied sample. Measurements were recorded following a one-minute stabilization period to ensure accurate readings.

*2.2.4.5. Scanning white light interferometer.* Gel tablets containing 1 % and 2 % furosemide were examined using scanning white light interferometry (SWLI) to evaluate their surface topography and micro-scale roughness, with the aim of understanding the influence of formulation composition — particularly surfactant concentration — on surface morphology. Measurements were captured using a Mirau-type interferometric objective at 10 × magnification, covering an area of approximately 700 × 500 μm. The acquired data were analysed in accordance with ISO 25,178 and ISO 21,920 surface roughness standards to provide a quantitative assessment of the printed surface quality.

*2.2.4.6. Microbial enumeration test and test for specific microorganisms.* Microbiological quality of the 1 % furosemide gel-based tablet formulation was assessed in accordance with the procedures outlined in the Ph. Eur. chapter 2.6.12 (Microbial Enumeration Tests) and 2.6.13 (Tests for Specified Microorganisms).

The total aerobic microbial count (TAMC) and total yeast and mold count (TYMC) were determined using the plate count method. Samples were appropriately diluted with sterile diluent and plated on casein soybean digest agar for TAMC and sabouraud dextrose agar for TYMC. Plates were incubated at 30–35 °C for bacterial counts and at 20–25 °C for fungal counts, following the incubation periods prescribed by Ph. Eur. guidelines.

In addition, testing for *Escherichia coli* was carried out using enrichment in selective broth followed by subculture on selective agar media, as described in Ph. Eur. 2.6.13. Results were expressed in colony-forming units (CFU) per gram of sample for enumeration, and the presence or absence of *E. coli* was confirmed in 1 g of the product. Acceptance criteria were based on Ph. Eur. requirements for oral non-sterile preparations: TAMC not exceeding $10^3$ CFU/g, TYMC not exceeding $10^2$ CFU/g, and the absence of *E. coli* in 1 g of sample.

**Table 1**
Accuracy of Micro-NIR model for furosemide BU in CuraBlend®.

| Method | Theoretical Level | Factor No | Mean BU [a] ( %) | Min ( %) | Max ( %) | SD ( %) | Deviation from Target ( %) |
|---|---|---|---|---|---|---|---|
| **HPLC** | 80 % | NA | 87.8 | 86.3 | 89.2 | 0.8 | NA |
| **Micro-NIR** | 80 % | 4 | 81.5 | 77.9 | 84.9 | 2.3 | −6.3 |
| **Method** | **Theoretical Level** | **Factor No** | **Mean BU [a] ( %)** | **Min ( %)** | **Max ( %)** | **SD ( %)** | **Deviation from Target ( %)** |
| **HPLC** | 100 % | NA | 101.6 | 99.1 | 105 | 2.1 | NA |
| **Micro-NIR** | 100 % | 4 | 95.0 | 92.3 | 97.9 | 2.3 | −6.7 |
| **Method** | **Theoretical Level** | **Factor No** | **Mean BU [a] ( %)** | **Min ( %)** | **Max ( %)** | **SD ( %)** | **Deviation from Target ( %)** |
| **HPLC** | 110 % | NA | 105.8 | 102.7 | 108.8 | 2.1 | NA |
| **Micro-NIR** | 110 % | 4 | 108.4 | 103.9 | 114.2 | 2.7 | 2.5 |

[a] Mean of 10 locations in syringe, $n = 10$.

#### 2.2.5. The stability studies

Batches of 1 % and 2 % furosemide formulations were produced and printed using the validated Pharma Printer® software at deposition weights ranging from 200 mg to 500 mg. Since the composition of each tablet size was identical and only the deposition weight varied, the 400 mg variant was selected as a representative strength for detailed characterization and stability studies.

Tablets were stored in Medi-Cup green Blisters® (Medi-Dose, USA), chosen for their compatibility and protective features. The packaging was sealed using the Roll-E-ZY Press, ensuring secure and tamper-evident closure. To evaluate the stability of both 1 % and 2 % furosemide formulations, a study was carried out at room temperature (21–25 °C) over predetermined time points: 0, 1, 3, and 6 months.

#### 2.2.6. Statistical analysis

All statistical analyses were performed using IBM SPSS Statistics (Version 30.0.0.0 (172), IBM Corp., Armonk, NY, USA). Dissolution data were expressed as mean ± standard deviation (SD) for six replicates per time point. An independent samples *t*-test was used to compare the percentage drug release between the 1 % and 2 % furosemide formulations at each individual time point (5, 10, 15, 20, 30, 45, and 60 min). For disintegration time comparison, a paired samples *t*-test was conducted to assess differences between the two formulations across matched tablets (n = 6). A significance level of $p < 0.05$ was considered statistically significant. Surface roughness data were presented descriptively due to the absence of replicate measurements.

## 3. Results

### 3.1. NIR-assisted production of blend uniformity in furosemide formulation

#### 3.1.1. Quantitative PLS NIR model parameters for built PLS models

The PLS model was built for furosemide using a calibration set of 131 samples at concentrations between 90 % and 110 %. The first derivative and standard normal variate (SNV) were applied for pretreatment methods. This model demonstrated good predictive performance with R2=0.91217, and root mean square error of calibration (RMSEC) of 3.37 %, and root mean square error of cross-validation (RMSECV) of 3.68 %. The scores plot (Fig. 4A) shows clustering of replicate samples and separation between concentration levels. These observations indicate the relevant spectral regions used for calibration and the ability of the model to distinguish concentration differences within the mixture.

The regression coefficient plot (Fig. 4B) displays peaks at 1404 nm and 1447 nm, corresponding to regions associated with C–H overtone and combination bands. These wavelengths are consistent with features observed in the pure furosemide API spectrum, with 1404 nm attributed to aromatic C–H and 1447 nm to aliphatic C–H vibrations. The homogeneity of NIR spectra across concentration levels confirms the consistency of spectral profiles (Fig. 5).

#### 3.1.2. External validation

The accuracy of the quantitative PLS NIR model for assessing BU of furosemide in CuraBlend® was evaluated across three independent batches with varying batch sizes: 50 g, 60 g, and 70 g (Table 1). For 80 % theoretical concentration, the mean content uniformity was 81.5 % with a standard deviation of 2.3 %. At the 100 % theoretical level, the mean content uniformity was 95.0 %, also with a standard deviation of 2.3 %. For the 110 % theoretical level, the mean content uniformity was 108.4 %, with a standard deviation of 2.7 %.

The precision test was conducted at three concentration levels (80 %, 100 %, and 110 %) using Factor 4. Measurements were repeated six times across ten samples at each concentration level. The average RSD % values were 1.4 % at 80 %, 1.0 % at 100 %, and 1.3 % at 110 %, indicating consistent precision across the tested range.

### 3.2. Assessment of within-syringe homogeneity during automated dosing

Content uniformity testing was conducted at the beginning, middle, and end of the printing process for both 1 % and 2 % furosemide formulations in CuraBlend®.

As shown in Table 2, both formulations maintain consistent API content across all printing stages. The average content values ranged from 97.6 % to 101.1 %, with low standard deviations and AVs of 4 (1 %) and 3 (2 %), respectively.

### 3.3. Quantitative analysis of drug content

Content uniformity for 1 % and 2 % furosemide formulations was evaluated across four tablet strengths (500 mg, 400 mg, 300 mg, and 200 mg) (Table 3). The analysis included the minimum, maximum, and mean content values, along with the AV, based on the criteria set by Ph. Eur. 2.9.40. The acceptance limits required content to fall within 85.0 % to 115.0 % of the labeled amount, with AV not exceeding 15. For all tablet strengths and concentrations, the mean drug content remained within the acceptable range. For instance, the 1 % furosemide 500 mg tablets had a mean content of 104.0 %, while the 2 % furosemide 500 mg tablets showed a mean of 107.6 %. AV values for all samples ranged

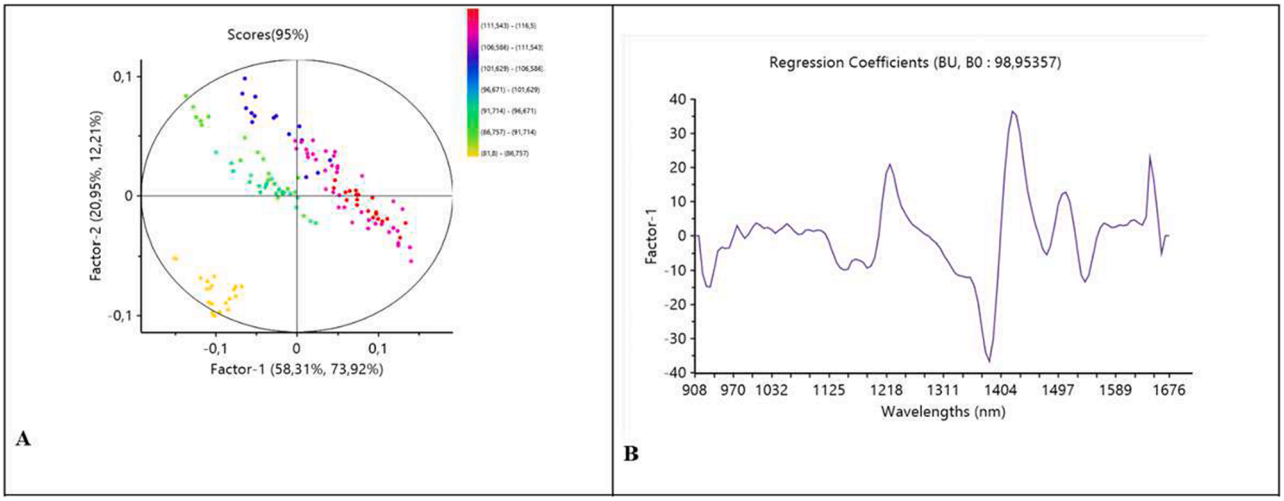


**Fig. 4.** (A) Scores plot for furosemide blend uniformity (BU) in CuraBlend® mixture ($n$ = 131 samples) and (B) Regression coefficients plot for furosemide BU in CuraBlend® mixture.

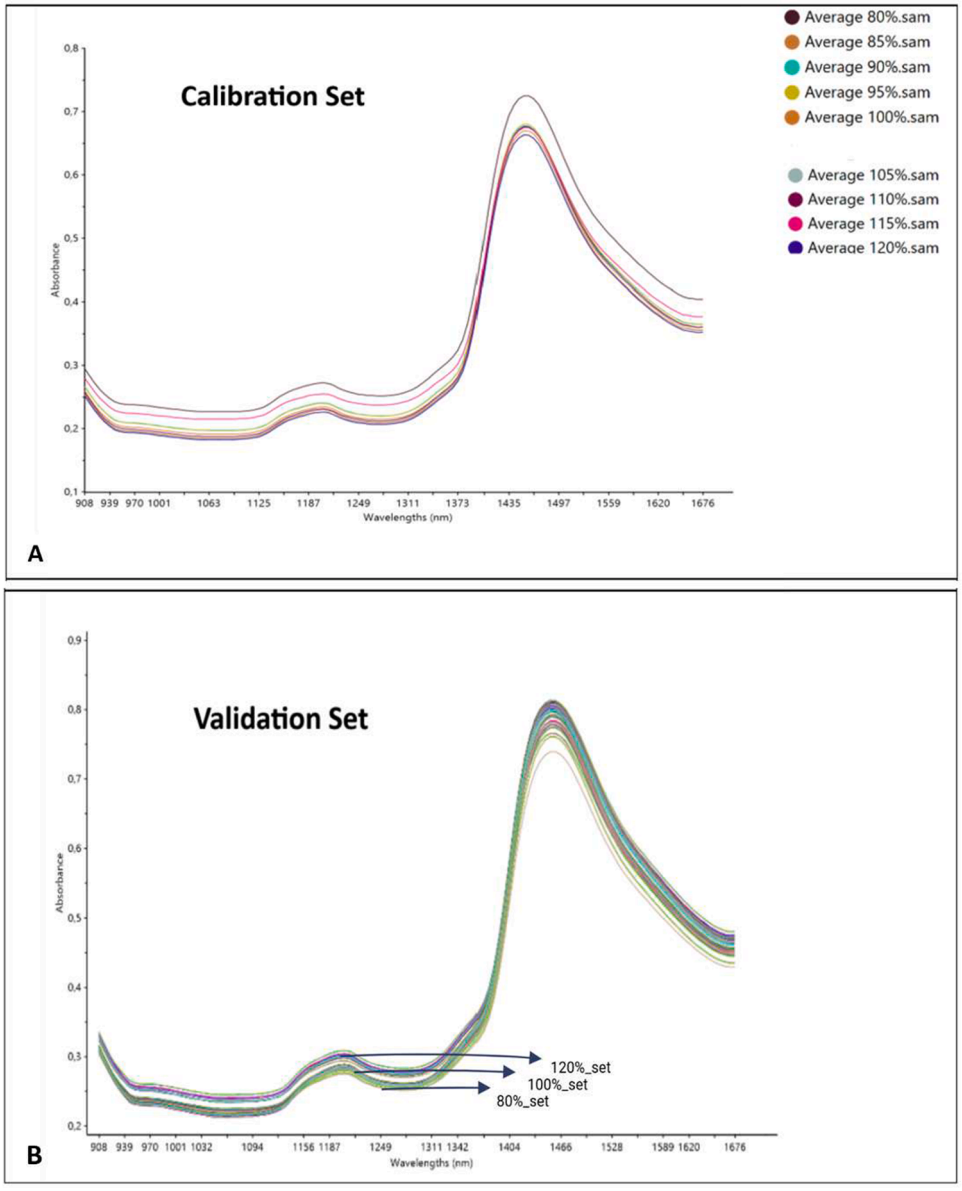


**Fig. 5.** Representative mean near-infrared (NIR) spectra of homogeneous batches at different theoretical concentration levels (80–120 %).

**Table 2**
Content uniformity results of syringe homogeneity test ($n = 10$).

| Product name | Printing Stage | API Content ( %) | Average ( %) ± SD | Acceptance Value |
|---|---|---|---|---|
| **1 % Furosemide** | Beginning of Printing | 98.0, 97.9, 97.6 | 97.9 ± 0.2 | 4 |
| | Mid-Point of Printing | 96.8, 97.3, 98.8 | 97.6 ± 1.0 | |
| | End of Printing | 101.3, 100.2, 99.6, 100.1 | 100.3 ± 0.7 | |
| **2 % Furosemide** | Beginning of Printing | 98.8, 99.5, 100.2 | 99.5 ± 0.7 | 3 |
| | Mid-Point of Printing | 100.1, 100.4, 100.5 | 100.3 ± 0.2 | |
| | End of Printing | 101.0, 100.6, 101.5, 102.6 | 101.1 ± 0.5 | |

from 4 to 10, complying with the required threshold. The minimum and maximum content values across all tablet sizes showed limited variation. For example, the 1 % 500 mg tablets ranged from 102.9 % to 106.0 %, and the 2 % 500 mg tablets from 106.5 % to 110.4 %. This consistency indicates uniform distribution of furosemide within the formulations across the different tablet sizes tested.

### 3.4. Disintegration time

Disintegration testing of 1 % and 2 % furosemide tablets across all sizes showed times under 10 min, meeting the Ph. Eur. requirement of ≤15 min for immediate-release tablets. These results confirm compliance with pharmacopoeial standards.

Additionally, a paired-sample *t*-test was conducted to compare the disintegration times of 1 % and 2 % furosemide formulations ($n = 6$ per formulation). The mean disintegration time for the 1 % formulation was

**Table 3**
Evaluation of dose uniformity in 1 % and 2 % furosemide formulations at multiple strengths ($n = 10$).

| Product Name | N | Minimum ( %) | Maximum ( %) | Mean ( %) | Acceptance Value (AV) |
|---|---|---|---|---|---|
| 1 % furosemide _200 mg | 10 | 103.6 | 111.0 | 106.1 | 10 |
| 1 % furosemide _300 mg | 10 | 104.1 | 107.2 | 106.3 | 7 |
| 1 % furosemide _400 mg | 10 | 103.7 | 109.0 | 106.2 | 9 |
| 1 % furosemide _500 mg | 10 | 102.9 | 106.0 | 104.0 | 4 |
| 2 % furosemide _200 mg | 10 | 106.4 | 111.6 | 108.2 | 10 |
| 2 % furosemide _300 mg | 10 | 104.5 | 109.3 | 107.2 | 9 |
| 2 % furosemide _400 mg | 10 | 105.3 | 109.0 | 107.2 | 9 |
| 2 % furosemide _500 mg | 10 | 106.5 | 110.4 | 107.6 | 9 |

7.78 ± 0.23 min, while the 2 % formulation showed a mean of 8.75 ± 0.19 min. A statistically significant difference was observed between the two formulations, $t(5) = -10.13$, $p < 0.001$. The 95 % confidence interval for the mean difference ranged from −1.21 to −0.72 min.

### 3.5. Water-based drug release assessment of furosemide gel tablets

The *in vitro* drug release profiles for three formulations, namely 400 mg 1 % furosemide, 400 mg 2 % furosemide, and the branded version were assessed at various time points (0, 5, 10, 15, 20, 30,45 and 60 min). The percentage of drug release was measured for each formulation at these time intervals.

The dissolution profile (Fig. 6) shows that the 1 % furosemide gel tablets released the drug more rapidly than the 2 % tablets, reaching over 80 % release within 30 min, while the 2 % tablets reached similar levels closer to 60 min. This indicates a faster dissolution rate for the lower-concentration formulation.

Statistical comparison of the dissolution profiles between the 1 % and 2 % Furosemide formulations demonstrated significant differences at all measured time points ($p < 0.05$) as shown in Table 4. During the initial 5–30 min, the 1 % formulation exhibited significantly higher drug release, whereas at 45 and 60 min, the 2 % formulation outperformed the 1 % in cumulative release. This suggests an initially faster dissolution for the 1 % formulation and a potentially more sustained release from the 2 % formulation.

### 3.6. Fourier-transform infrared spectroscopy evaluation of API-excipient interactions in furosemide tablets

FTIR analysis was conducted to obtain the infrared spectra of CuraBlend® as the excipient base, furosemide as API, and the extruded furosemide tablets. The purpose of the analysis was to compare the FTIR spectra of furosemide in its powder form and within the tablet formulation, aiming to identify any variations in peak characteristics that may provide insight into formulation compatibility and quality control. Fig. 7 presents the FTIR spectra of furosemide powder, extruded tablets (CuraBlend gel tablet – pure CuraBlend mixture extruded tablet without API; furosemide tablet – extruded tablet with 1 % and 2 % furosemide content), and main components of the CuraBlend mixture (Cocoa butter and Xylitol).

The FTIR spectrum of pure furosemide (bottom trace in Fig. 7) exhibits distinct absorption bands characteristic of its molecular structure, including strong peaks near 3400 $cm^{-1}$ (N–H and O–H stretching), 1680 $cm^{-1}$ ($C = O$ stretching), and multiple bands in the fingerprint region (600–1600 $cm^{-1}$) corresponding to aromatic and sulfonamide groups (Bolukbasi and Yilmaz, 2012; Gallignani et al., 2014). The spectrum of cocoa butter (top trace) is dominated by strong C–H stretching vibrations around 2850–2950 $cm^{-1}$ and carbonyl stretching near 1740 $cm^{-1}$, while xylitol shows prominent O–H stretching and C–O stretching bands (Bresson et al., 2021; Matawo et al., 2020; Roostar et al., 2025). Cocoa butter and xylitol were specifically included as reference excipients, since they are key components of the CuraBlend® base.

The CuraBlend® gel tablet base (without API) displays a broad O–H stretching band and characteristic excipient peaks but lacks the distinctive furosemide bands. In the spectra of extruded tablets containing furosemide (Fu 1 % + PS 1 % 1 d, Fu 2 % + PS 2.6 % 1 d, Fu 2 % + PS 2 % 1 w, and Fu 2 % + PS 2 % 3 m), the key furosemide peaks-particularly those at 3400 $cm^{-1}$, 1680 $cm^{-1}$, and in the fingerprint region-are preserved, although their intensity is reduced and some peak broadening is observed compared to the pure drug. This attenuation and broadening are attributed to the dilution of furosemide within the excipient matrix and overlap with excipient absorption bands.

### 3.7. XRPD characterization of furosemide and excipient components in gel-based tablets

XRPD analysis was conducted on the semi-solid CuraBlend® base as well as individual solid ingredients from the formulation, such as xylitol, and furosemide. Fig. 8 presents the XRD patterns for furosemide powder, CuraBlend excipients mixture, main component of the mixture, and the extruded tablets with 1 % and 2 % of furosemide in different time points.

X-ray diffraction patterns of pure furosemide powder exhibited characteristic sharp peaks at 2θ values of approximately 6°, 12°, 18°,

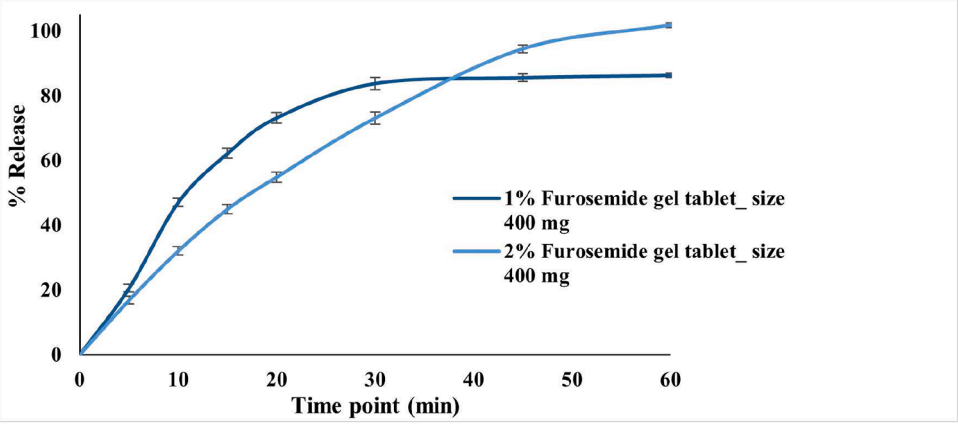


**Fig. 6.** Dissolution profile of furosemide 400 mg gel tablets: 1 %, 2 %, $n = 6$ tablets.

**Table 4**
Comparison of Mean % Drug Release Between Furosemide 1 % and 2 % Formulations at Different Time Points ($n = 6$ per group).

| Timepoint (min) | Mean % Release (1 %formulation) | Mean % Release (2 % formulation) | Mean Difference | *p-value | Significance |
|---|---|---|---|---|---|
| 5 | 20.53 ± 3.21 | 16.85 ± 1.15 | 3.68 | 0.024 | Yes |
| 10 | 47.00 ± 2.00 | 32.00 ± 1.30 | 15.00 | <0.001 | Yes |
| 15 | 62.10 ± 1.70 | 44.90 ± 1.50 | 17.20 | <0.001 | Yes |
| 20 | 73.10 ± 1.50 | 54.80 ± 1.60 | 18.30 | <0.001 | Yes |
| 30 | 83.70 ± 1.30 | 73.00 ± 1.90 | 10.70 | 0.001 | Yes |
| 45 | 85.50 ± 0.90 | 94.40 ± 1.20 | −8.90 | 0.003 | Yes |
| 60 | 86.20 ± 0.90 | 101.70 ± 0.70 | −15.50 | <0.001 | Yes |

* p-values derived from independent samples *t*-tests.

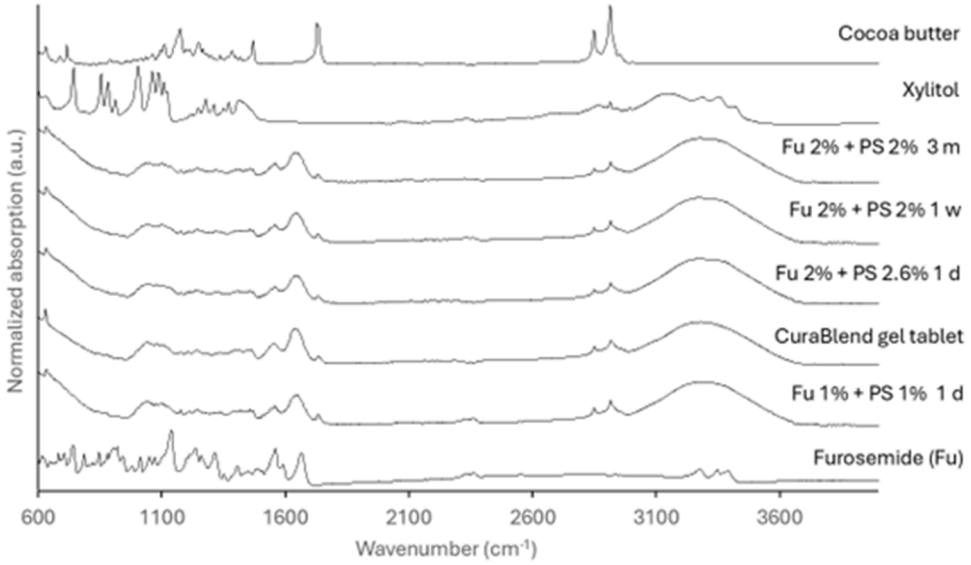


**Fig. 7.** Fourier-transform infrared (FTIR) spectra of extruded furosemide gel tablets at different time points, pure furosemide powder, CuraBlend® base and individual spectra of some base components.
Key: d, day; Fu, furosemide; m, month; PS, polysorbate 80; w, week.

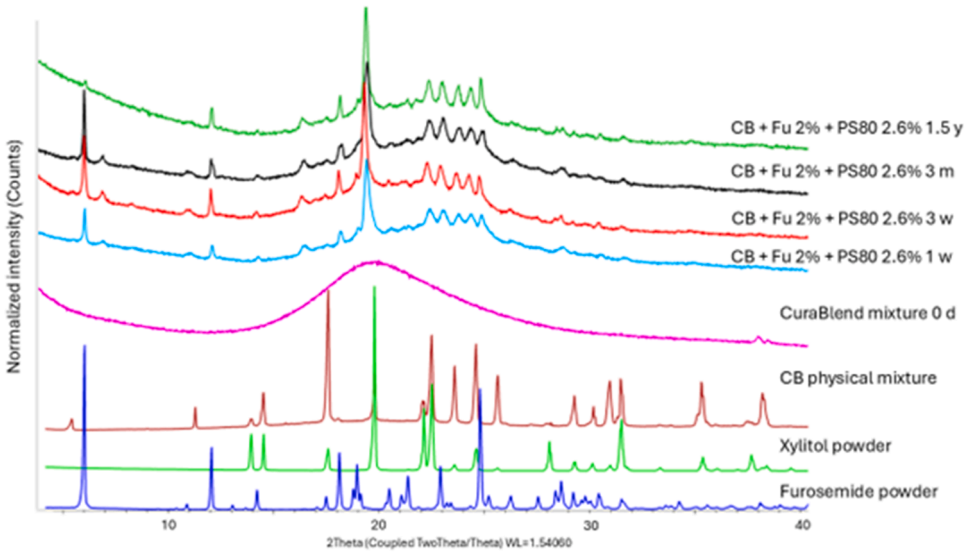


**Fig. 8.** X-ray Powder Diffraction (XRPD) patterns of 2 % furosemide extruded gel tablets at different time points and pure furosemide powder, CuraBlend® base and physical mixture of solid components.
Key: CB, CuraBlend®; CB dry mixture, physical mixture of solid CuraBlend® base components; d, day; Fu, furosemide; m, month; PS80, polysorbate 80; w, week; y, year.

19°, and 25° (Fig. 8, bottom blue pattern), confirming its highly crystalline nature (Aceves et al., 2000; Adrjanowicz et al., 2011; Bolukbasi and Yilmaz, 2012) . In contrast, the CuraBlend® base displayed a predominantly amorphous pattern with a broad halo (Fig. 8, pink pattern), while the physical mixture, the pattern of pure cocoa butter (not shown in the figure) and xylitol powder showed distinct crystalline patterns that differed from furosemide (Bresson et al., 2021; Colella et al., 2023; Matawo et al., 2020). The extruded formulation containing 2 % furosemide and 2.6 % polysorbate 80 preserved the major characteristic peaks of furosemide across all time points, with the most prominent peak at approximately 6° 2θ remaining clearly visible even after 1.5 years of storage (Fig. 8, upper patterns). However, minor changes in peak intensity and shape were observed over time, including slight broadening in the 3-month and 1.5-year samples. These alterations may reflect weak physical interactions between furosemide and the excipient matrix or partial reorganization of the microstructure, rather than major crystalline transitions.The more visible peak at 20° 2θ, which is already distinct in gel tablets that have been standing for a week, comes from xylitol (Fig. 8, bottom light green pattern).

Concentration-dependent effects of both furosemide and polysorbate 80 on the XRD patterns are illustrated in Fig. 9. The formulation containing 1 % furosemide with 1 % polysorbate (light blue pattern) exhibited reduced intensity of drug-related peaks compared to formulations with 2 % furosemide, reflecting the lower drug concentration. Among furosemide formulations, varying polysorbate concentrations (1 %, 2 %, and 2.6 %) did not appear to significantly influence the preservation of the crystalline structure, as the X-ray diffraction patterns remained largely consistent across samples. However, the less distinct furosemide peaks in the 1 % polysorbate formulation may be influenced by both the amorphous halo of the CuraBlend® matrix and potential weak drug-excipient interactions. Furthermore, since measurements were taken one week after preparation, observed changes might reflect early-stage physical transitions in the matrix, such as excipient reorganization or phase behavior shifts.

The temporal stability of the 2 % furosemide formulation with 2.6 % polysorbate (Fig. 8) demonstrates that while peak intensities show slight variations over time, the essential crystalline fingerprint of furosemide remains intact. Nonetheless, the spectral variations observed in excipient-related regions—particularly in the lower 2θ range (5–15°) and 20–25° 2θ— may indicate reorganization or crystallization of components like cocoa butter and xylitol during storage. These findings suggest that while no major crystallinity loss occurs in furosemide, subtle matrix-related effects and potential weak interactions cannot be ruled out. Xylitol is known to rapidly crystallize on the tablet surface after cooling, while cocoa butter undergoes polymorphic transitions over time, both of which may affect the diffraction and spectral patterns. Comparative analysis of the different formulations in Fig. 9 reveals that higher drug loading (2 % vs. 1 %) results in more prominent furosemide peaks, while higher polysorbate concentrations appear to enhance peak definition. Overall, while no significant disruption of furosemide's crystalline structure was evident, observed differences are now interpreted as likely resulting from a combination of matrix effects, storage-related transformations, and possible weak interactions within the formulation.

### 3.8. Surface topography evaluation of furosemide gel tablets via SWLI

Surface characterization of 3D-printed gel tablets containing furosemide was performed using SWLI to evaluate the impact of both API concentration and the presence of a surfactant (polysorbate 80). The formulations analysed included a 1 % w/w furosemide tablet with polysorbate 80 (1 % w/w) and a 2 % w/w furosemide tablet containing 2.0 % w/w polysorbate 80. In the 1 % furosemide tablet, topographic mapping (Fig10.A1) revealed a relatively rough and uneven surface, with a root mean square height (Sq) of 2.074 μm, a maximum height (Sz) of 35.76 μm, and an arithmetical mean height (Sa) of 1.498 μm. These values are indicative of a coarse surface texture with multiple moderate-level peaks and valleys.

The corresponding surface roughness map (Fig10.A2) and profile (Fig10.A3) provided additional metrics following ISO 21,920 standards. The arithmetic mean roughness (Ra) was measured at 0.68 μm, while the root mean square roughness (Rq) was 0.86 μm. The maximum roughness height (Rz) was 5.50 μm, and the surface exhibited negative skewness (Rsk = –0.44), indicating a tendency toward valley-dominated morphology. The kurtosis (Rku) of 4.73 suggests a relatively normal distribution with some sharp surface features. In contrast, the 2 % furosemide tablet containing 2.0 % PS80 displayed a notably smoother average surface in the topographic map (Fig. 10.B1), with Sq = 1.434 μm, Sa = 0.93 μm, and Sz = 46.69 μm. Despite the reduced average roughness values, the maximum height (Sz) was actually higher than in the 1 % formulation, indicating deeper localized valleys or more pronounced structural features. The roughness map and surface profile (Fig. 10.B21& B3) showed Ra = 0.68 μm and Rq = 1.43 μm, values that are comparable in magnitude to those seen in the 1 % formulation.

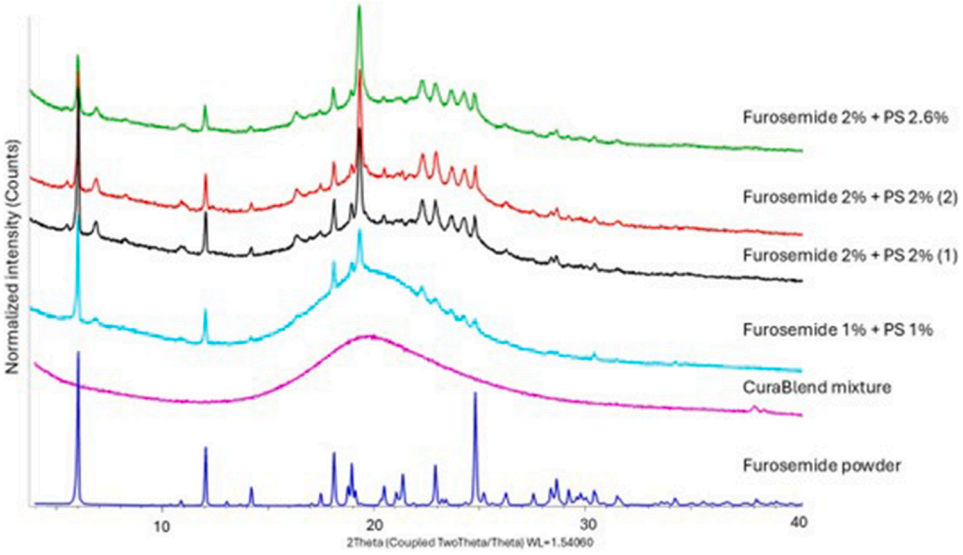


**Fig. 9.** X-ray Powder Diffraction (XRPD) patterns of furosemide extruded gel tablets with different furosemide and polysorbate 80 contents.
Key: CuraBlend mixture, base without API at zero time point; PS, polysorbate 80 (1 and 2 indicate different batches with the same composition).

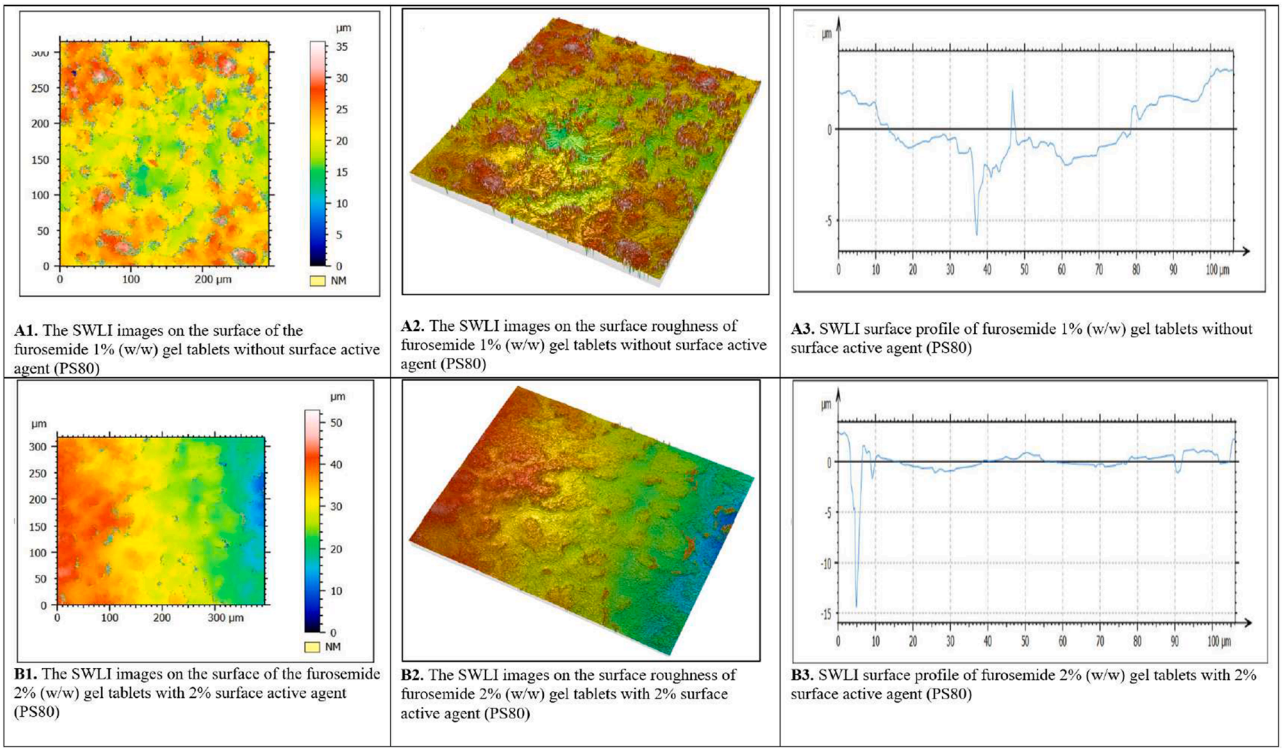


**Fig. 10.** Scanning White Light Interferometry (SWLI) topography, surface roughness maps, and profiles of furosemide gel tablets with polysorbate 80,$n = 1$
A1. SWLI topography images of 1 % (w/w) furosemide gel tablets with 1.0 % (w/w) PS80. Surface parameters (ISO 25,178): $Sq = 2.074$ μm (root mean square height), $Sz = 35.76$ μm (maximum height), $Sa = 1.498$ μm (arithmetical mean height).
A2 & A3. SWLI surface roughness image (A2) and profile (A3) of 1 % (w/w) furosemide gel tablets with 1.0 % PS80. Roughness parameters (ISO 21,920): $Rq = 0.86$ μm (root mean square roughness), $Rsk = -0.44$ (skewness), $Rku = 4.727$ (kurtosis), $Rz = 5.50$ μm (mean peak-to-valley height), $Ra = 0.6761$ μm (arithmetical mean roughness).
B1. SWLI topography images of 2 % (w/w) furosemide gel tablets with 2.0 % PS80. Surface parameters (ISO 25,178): $Sq = 1.43$ μm, $Sz = 46.69$ μm, $Sa = 0.93$ μm.
B2 & B3. SWLI surface roughness image (B2) and profile (B3) of 2 % (w/w) furosemide gel tablets with 2.0 % PS80. Roughness parameters: $Rq = 1.43$ μm, $Rsk = -3.38$, $Rku = 23.51$, $Rz = 12.93$ μm, $Ra = 0.68$ μm.
**Abbreviations:** SWLI = Scanning White Light Interferometry; PS80 = Polysorbate 80; Sq = root mean square height; Sa = arithmetical mean height; Sz = maximum height; Rq = root mean square roughness; Ra = arithmetical mean roughness; Rsk = skewness; Rku = kurtosis; Rz = mean peak-to-valley height.

However, the Rz value increased substantially to 12.93 μm, and the Rsk dropped sharply to –3.38, suggesting a significant presence of narrow valleys. Additionally, Rku increased dramatically to 23.51, reflecting a more peaked or spiked distribution of surface height data, which may influence texture perception or functional surface behavior.

### 3.9. Stability study

A six-month stability study was performed on two 3D-printed gel-based furosemide tablet formulations, containing 1 % and 2 % of the active ingredient, each at 400 mg strength. The tablets were stored under ambient conditions in Medi-Cup Blisters and evaluated at baseline, and after one, three, and six months (Table 5). The study assessed visual appearance, pH, assay, dissolution, and microbiological quality, in alignment with regulatory expectations including (ICH Q2(R2): Validation of Analytical Procedures, 2003).

Throughout the study, both formulations maintained acceptable physical appearance, consistent with the specification of off-white, soft chewable tablets with vanilla flavor. No visual signs of physical degradation such as discoloration, spotting, or shape deformation were observed at any time point. pH values for both formulations remained below the specification limit of 6.0 during the entire study period. For the 1 % formulation, the pH values ranged from 4.8 to 4.9, while the 2 % formulation showed a slight fluctuation from 4.9 to 5.0 and then to 4.8 by six months. These variations were minor and remained within acceptable limits for the gel-based matrix system. Assay values were within the defined range of 90.0–110.0 % for both formulations over the entire study period. The 1 % furosemide formulation showed a decrease from 107.8 % at baseline to 104.8 % at six months, representing a 3.0 % reduction. The 2 % formulation declined from 105.6 % to 102.4 %, reflecting a change of 3.2 % (Fig. 11). As neither formulation exhibited a change exceeding 5 %, these variations are not considered significant under ICH Q1A (R2) guidelines and indicate acceptable potency retention during the six-month storage period.

Dissolution performance was initially above the required threshold for immediate-release dosage forms, which, for a Q value of 80 %, requires a minimum of 85 % dissolution in 60 min at Stage 1 testing. At baseline, the 1 % formulation showed 86.2 % ± 0.9 %, while the 2 % formulation exhibited 101.7 % ± 0.7 %. By the sixth month, the dissolution rate of the 2 % formulation had decreased to 88.5 %, which remains within the acceptable range. However, the 1 % formulation showed a decline to 76.3 % ± 1.7 %, falling below the Stage 1 threshold (Fig. 11). This reduction may reflect a potential concern with drug release over time, suggesting the need for Stage 2 dissolution testing as outlined in pharmacopeial guidance. Nevertheless, it's important to note that these formulations are gel tablets designed to be partially chewed or allowed to melt in the mouth, and therefore, conventional dissolution testing may not fully reflect their *in vivo* performance. Microbiological testing was performed on the 1 % formulation, including TAMC, TYMC, and *Escherichia coli*. Results showed consistent microbial quality across all tested time points. Total aerobic microbial counts and yeast and mold counts remained below 10 CFU/g, and *E. coli* was absent in all samples, confirming compliance with microbiological safety requirements.

**Table 5**
Stability report of 1 % and 2 % furosemide gel-based tablets.

| Test | Specification | Time 0 | 1 Month | 3 Month | 6 Month |
|---|---|---|---|---|---|
| 1 % furosemide gel tablet | | | | | |
| Appearance | Off-white, soft chewable tablet with vanilla flavour | Conforms | Conforms | Conforms | Conforms |
| pH ($N = 3$ tablets) | ≤6.0 | 4.8 | 4.8 | 4.6 | 4.9 |
| Assay ($N = 5$ tablets) | 90.0–110.0 % | 107.8 % | 106.7 % | 105.3 % | 104.8 % |
| Dissolution ($N = 6$ tablets) | $Q = 80$ of Furosemide in 60 min | 86.2 % ± 0.9 % | – | – | 76.3 % ±1.7 % |
| TAMC | NMT $10^3$ CFU/g | <10 CFU/g | <10 CFU/g | <10 CFU/g | <10 CFU/g |
| TYMC | NMT $10^2$ CFU/g | <10 CFU/g | <10 CFU/g | <10 CFU/g | <10 CFU/g |
| *Escherichia coli* | Absence in 1 g | Not detected | Not detected | Not detected | Not detected |
| 2 % furosemide gel tablet | | | | | |
| Appearance | Off-white, soft chewable tablet with vanilla flavour | Conforms | – | Conforms | Conforms |
| pH ($N = 3$ tablets) | ≤6.0 | 4.9 | – | 5.0 | 4.8 |
| Assay ($N = 5$ tablets) | 90.0–110.0 % | 105.6 % | – | 104.5 % | 102.4 % |
| Dissolution ($N = 6$ tablets) | $Q = 80$ of Furosemide in 60 min | 101.7 % ± 0.7 % | – | – | 88.5 % |

N: number, CFU: Colony-Forming Unit.

## 4. Discussion

This study demonstrates the successful integration of SSE 3D printing using the CSS technology with advanced in-process and post-process quality control for the personalized manufacture of pediatric furosemide tablets. By combining real-time BU monitoring using NIR spectroscopy and chemometric modeling, precise in-process weight control, and thorough pharmacopeial testing-including content uniformity, dissolution, disintegration, and microbiological quality-we established a robust and reproducible workflow. Solid-state analyses (XRD, FTIR) confirmed the chemical and physical stability of furosemide within the gel matrix, while surface topography evaluation via SWLI further validated the uniformity and quality of the 3D-printed tablets.

### 4.1. Furosemide NIR model analysis

The evaluation of the furosemide BU model further demonstrated the efficacy of the PLS regression approach. The calibration set achieved high $R^2$ values (0.97–0.99) with RMSEC values as low as 0.42 %, indicating good predictive performance. This corroborates findings from previous studies where the inclusion of diverse calibration sets improved predictive performance (Baratieri et al., 2006; Mantanus et al., 2009).

The adoption of NIR spectroscopy in pharmaceutical manufacturing represents a paradigm shift towards sustainable, efficient, and patient-centric practices. By focusing on BU monitoring within semi-solid formulations during 3D printing, this study aligns with the broader goals of continuous manufacturing. Variations in BU have significant implications for dose accuracy and therapeutic efficacy, particularly in personalized medicine where small batch sizes and rapid adjustments are required (Foo et al., 2018).The strong correlation between corrected NIR predictions and HPLC values reinforces the feasibility of replacing traditional methods with non-destructive alternatives. The integration of NIR spectroscopy aligns with ICH Q2 guidelines, which emphasize accuracy, precision, and linearity in method validation (Blanco and Alcalá, 2006). Previous studies on NIR applications in solid dosage forms, creams, and capsules validate its versatility across pharmaceutical matrices (Paris et al., 2006; Wang et al., 2010).This study extends the application to semi-solid pharmaceutical excipient bases or inks, a novel area, underscoring the methodology's adaptability and relevance. The portability and ease of integration of NIR spectroscopy further enhance its applicability for at-line use in both manufacturing and clinical settings. This capability aligns with industry trends favoring real-time monitoring technologies to streamline production and improve patient outcomes (Yang et al., 2023). Addressing inconsistencies in BU at the earliest stages of the manufacturing process reduces risks associated with dose variability, ensuring patient safety and therapeutic efficacy.

Sampling and the selection of appropriate sampling accessories play a critical role in ensuring accurate and reliable NIR spectroscopy measurements. Representative sampling is especially vital when analysing heterogeneous materials, such as polymer pellets, where consistent measurement of the bulk sample is required. Accessories like Sample Cup Spinners are particularly effective in improving representativeness

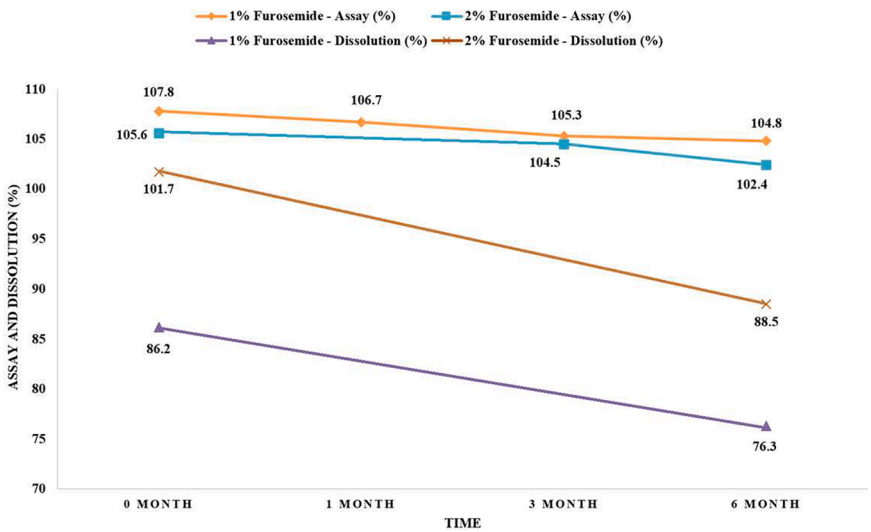


**Fig. 11.** Long-term stability of furosemide gel tablets: Assay and dissolution trends.

and efficiency in such contexts (Pasquini, 2018). In industrial applications, the integration of sampling accessories with in-line or at-line NIR systems further enhances process control by enabling real-time monitoring and reducing dependency on laboratory-based analyses (Soriano et al., 2019). Additionally, the use of autosamplers has proven to be cost-effective and time-efficient, making NIR spectroscopy a practical tool for routine applications (Workman and Weyer, 2007). However, there are significant challenges associated with NIR sampling and its accessories. Many commercial NIR sampling accessories are primarily designed for laboratory settings, requiring technical expertise that may not be readily available in industrial environments (Soriano et al., 2019). Ensuring reproducibility and accuracy in measurements is another critical concern, especially in the analysis of granular samples where non-fully interacted radiation can lead to variability. While innovations such as diffusers can improve measurement reliability, challenges persist when detecting low-content analytes, as the sensitivity and detection limits are heavily influenced by the choice of accessory (Roggo et al., 2007; Simpson, 2005). To address these challenges, the development of rugged and operator-friendly sampling units, as well as advanced accessories like droplet collars and modified reflectance tools, offers promising solutions to enhance NIR analysis in diverse settings (Sarraguça and Lopes, 2009).

Future research should focus on expanding calibration models to include a wider range of pharmaceutical excipient bases and APIs. Additionally, real-world application of at-line and on-line NIR spectroscopy in clinical settings could provide insights into its scalability and operational feasibility. Developing standardized protocols for calibration and validation will further enhance the adoption of this technology, ensuring compliance with regulatory standards while maximizing its impact on pharmaceutical manufacturing. However, several challenges must be addressed to fully realize the potential of NIR spectroscopy. For instance, the technique is highly sensitive to sample heterogeneity, which can lead to variability in measurements, especially for low-content analytes or complex matrices (Blanco et al., 2007; Roggo et al., 2007). Additionally, the initial cost of NIR instrumentation and the need for frequent calibration updates can be barriers to widespread adoption, particularly for small-scale manufacturers (Sarraguça and Lopes, 2009). Furthermore, the interpretation of NIR spectra often requires advanced chemometric expertise, which may not be readily available in all settings (Pasquini, 2018).

### 4.2. Syringe homogeneity

The results of the within-syringe homogeneity assessment clearly demonstrate the robustness and reliability of the automated dosing process for both 1 % and 2 % furosemide formulations. The observed API content remained consistent across all stages of the printing cycle, with minimal variability and low acceptance values. This level of uniformity is essential for the production of individualized medicines, where precise dosing is critical for therapeutic efficacy and safety.The low standard deviations observed in both formulations suggest that the CuraBlend® excipient system effectively maintains a uniform suspension of furosemide throughout the extrusion and printing process. This is particularly important for semi-solid and gel-based formulations, where phase separation or settling of the API could otherwise lead to dose variability. Furthermore, the acceptance values of 3 and 4 for the 2 % and 1 % formulations, respectively, are well within the acceptable range defined by pharmacopeial standards, underscoring the suitability of the process for routine pharmaceutical manufacturing. The lack of significant differences in API content between the start and end of the printing process also suggests that the system can reliably produce multiple units in succession without the need for frequent recalibration or intervention.

### 4.3. Content uniformity across tablet strengths

Ensuring content uniformity is critical for the efficacy and safety of pharmaceutical tablets. Our analysis of 1 % and 2 % furosemide formulations across tablet strengths (200 mg to 500 mg) as shown in Fig. 12 revealed mean drug content values within the acceptable range of 85.0 % to 115.0 %, as stipulated by Ph. Eur. 2.9.40. The AV for all samples were below the threshold of 15, indicating consistent drug distribution. These results are consistent with previous studies (Sandler Topelius et al., 2024; Shokraneh et al., 2025) which emphasized the importance of uniformity in dosage units for therapeutic effectiveness. Similar findings have also been reported in studies evaluating 3D-printed and compounded pediatric dosage forms (Lafeber et al., 2021; Van Der Zanden et al., 2021).

### 4.4. Surface topography evaluation

The SWLI analysis highlighted formulation-dependent differences in surface morphology between the 1 % and 2 % furosemide tablets. The 1 % formulation (with 1 % PS80) exhibited higher average roughness values (Sq = 2.07 μm; Sa = 1.49 μm) and lower extreme height features (Sz = 35.76 μm; Rz = 5.50 μm), indicating a uniformly coarse but balanced surface. Negative skewness (Rsk = –0.44) and moderate kurtosis (Rku = 4.73) support a slightly valley-dominant yet consistent surface profile.

In contrast, the 2 % formulation with 2 % PS80 showed reduced average roughness (Sq = 1.43 μm; Sa = 0.93 μm) but greater surface extremes (Sz = 46.69 μm; Rz = 12.93 μm), as well as highly negative skewness (Rsk = –3.38) and elevated kurtosis (Rku = 23.51). These metrics point to a morphology dominated by narrow, deep valleys and sharp surface peaks. Such microstructural differences likely stem from altered rheological or phase behavior at higher surfactant and API concentrations, influencing drying patterns and surface solidification during printing.

The observed topographical differences may help explain the variations in early dissolution behavior and disintegration kinetics between formulations. Surfaces with more uniform texture may promote faster and more consistent disintegration, while highly spiked morphologies with deep valleys might delay wetting or tablet erosion. Importantly, these findings underline the utility of SWLI for guiding formulation development, as surface texture can serve not only as a fingerprint of print quality but also as a tunable parameter affecting performance.

While SWLI has been widely used in microelectronics and optics for high-precision surface analysis, its application in pharmaceutical research is only emerging (Coupland and Lobera, 2010; Kassamakov et al., 2007; O Mahony et al., 2003). Recent studies have demonstrated SWLI's potential for characterizing surface roughness in pharmaceutical films and nanofibrous mats (Genina et al., 2012; Paaver et al., 2014), as well as for quality assurance of printed drug delivery systems (Sandler et al., 2014). In this study, we applied SWLI to evaluate the surface topography of semi-solid extruded, 3D-printed furosemide tablets-a novel approach in the context of pediatric personalized medicines. Our results revealed formulation-dependent differences in surface roughness and morphology, providing new insights into how excipient composition and process parameters influence the physical properties of the final dosage form. By leveraging SWLI's non-contact, high-resolution imaging, we were able to quantitatively assess surface uniformity and layer integrity without sample preparation or risk of altering delicate structures. This complements our comprehensive quality control strategy, which also included BU monitoring by NIR spectroscopy, in-process weight control, and pharmacopeial testing for content, dissolution, and microbiological quality. Moreover, these findings suggest that surface texture parameters can be used not only as a fingerprint for product quality, but also as tunable targets during formulation development to achieve desired disintegration and release profiles. The integration of SWLI into our workflow not only supports a Quality by Design approach

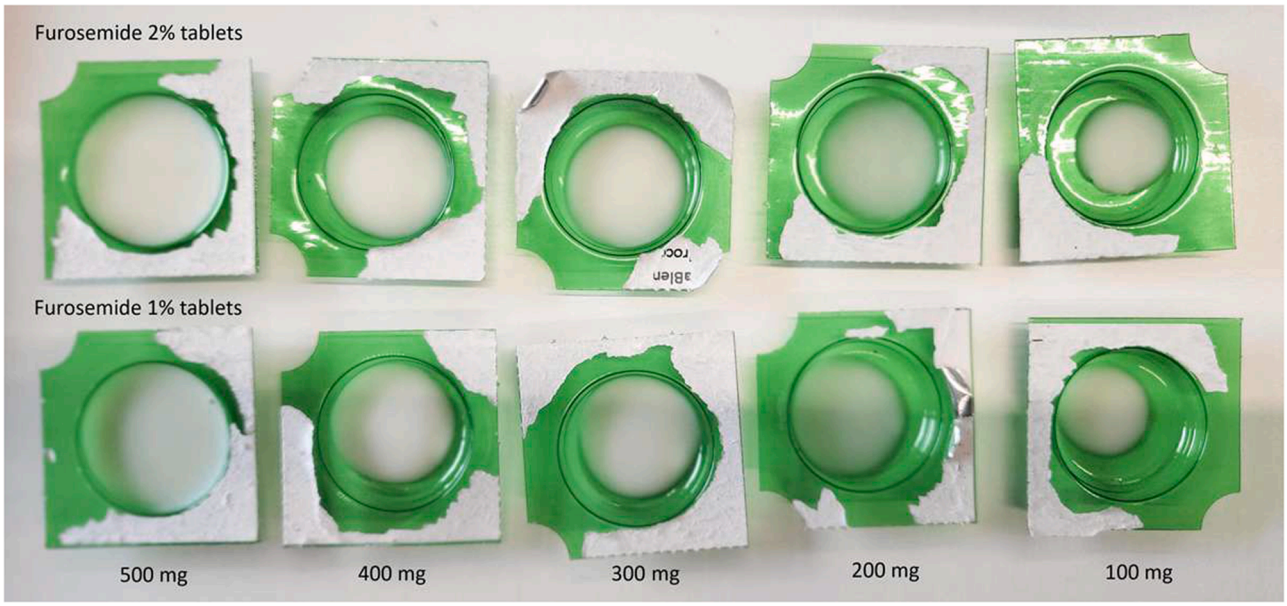


**Fig. 12.** Images of 1 % and 2 % furosemide gel tablets at deposition weights ranging from 100 mg to 500 mg.

(Paaver et al., 2014) but also enhances our ability to optimize and assure the consistency of advanced, patient-specific pharmaceutical products. In addition, surface properties may be optimized during formulation development by adjusting excipient ratios, surfactant concentration, and process parameters such as extrusion temperature and flow rate. These factors influence surface roughness, uniformity, and feature geometry—key characteristics that can affect disintegration, mouthfeel, and drug release.

### 4.5. Disintegration time

Disintegration testing revealed that all tablet sizes, for both 1 % and 2 % furosemide formulations, disintegrated in under 10 min. This performance complies with the Ph. Eur. requirement for immediate-release tablets, which mandate disintegration within 15 min. Rapid disintegration is crucial for ensuring timely drug release and onset of action, particularly in immediate-release formulations. The observed disintegration times are consistent with those reported in similar studies evaluating immediate-release tablet formulations (Khaled et al., 2015). In addition to excipient composition, surface morphology may also contribute to disintegration behavior. The SWLI test results revealed distinct differences in surface texture between the formulations, particularly in terms of Rsk and Rku. The 1 % formulation exhibited a relatively uniform surface with moderate valleys (Rsk = –0.44), while the 2 % formulation showed much deeper and sharper surface depressions (Rsk = –3.38; Rku = 23.51). These valley-rich, spiked surface profiles may enhance media penetration and accelerate matrix breakdown, supporting the observed disintegration performance. Together, these results suggest that surface architecture—quantified through high-resolution topographical analysis—can meaningfully influence disintegration kinetics alongside formulation composition.

### 4.6. Dissolution profiles and drug release

The dissolution behavior of furosemide tablets is pivotal for their bioavailability. Our *in vitro* dissolution studies demonstrated that both 1 % and 2 % formulations met the required dissolution criteria at initial time points. However, a notable decline in the dissolution rate of the 1 % formulation was observed at the six-month mark, falling below the 80 % threshold within 60 min. Furosemide's classification as a BCS class IV compound (Granero et al., 2010) highlights its inherent challenges for oral therapy, as it possesses both low aqueous solubility and limited intestinal permeability. These properties often result in poor and variable bioavailability when administered in conventional forms. In our work, the use of semi-solid extrusion 3D printing enabled the incorporation of furosemide into a solid dispersion within a hydrophilic excipient matrix, a strategy known to enhance the dissolution rate of poorly soluble drugs. The rapid dissolution observed in our formulations-exceeding 85 % drug release within 15 min for all freshly prepared tablets-suggests that this approach effectively improves the drug's release characteristics. Notably, the addition of polysorbate 80 as a surfactant in our matrix may further support drug absorption by enhancing both wettability and membrane permeability (Lafeber et al., 2021). Moreover, the SWLI surface characterization supports this observation. The higher Rku and more negative Rsk values seen in the 2 % formulation indicate the presence of sharp valleys and heterogeneous surface features. These may enhance the wettability and effective surface area of the tablet, facilitating improved penetration of the dissolution medium and contributing to the more complete and sustained drug release profile. This suggests that surface topography plays a complementary role alongside formulation composition in modulating the dissolution behavior.

The 2 % formulation demonstrates a more sustained but eventually more complete release, reaching over 95 % release at 60 min, while the 1 % formulation reaches approximately 85 % and plateaus earlier. The plateauing of the 1 % furosemide formulation's dissolution profile at approximately 85 % may be attributed to time-dependent saturation effects within the dissolution medium. Furosemide, a BCS Class IV drug, is characterized by low aqueous solubility, and the relatively limited amount of surfactant (1 % w/w PS80) in the lower concentration formulation may have been insufficient to fully maintain drug solubilization during the test. As a result, local saturation may have occurred early, reducing the concentration gradient and slowing further dissolution. In contrast, the 2 % formulation, which contained a higher PS80 concentration (2 % w/w), demonstrated both enhanced wettability and solubilization capacity, enabling a more sustained and complete release. This behavior aligns well with the SWLI surface characterization data, the 2 % formulation with 2 % PS80 exhibited a smoother average surface (Sq = 1.434 μm) but with sharper localized features (Rku = 23.51, Rz = 12.93 μm), likely due to microphase domains formed during extrusion. These surface irregularities may have increased the effective surface area or altered wettability, promoting more efficient penetration of the

dissolution medium and facilitating enhanced and prolonged drug release in the 2 % formulation. The highly negative skewness (Rsk = −3.376) also supports the idea of valleys that trap liquid, aiding matrix erosion and sustained release.

This relationship between surface topography and dissolution kinetics is consistent with mechanistic insights from crystal surface science. A recent study by Li et al. (2023) emonstrated that heterogeneous and discontinuous dissolution behavior arises from localized surface features such as etch pits and step waves, which create dynamically shifting zones of reactivity. Although their work focused on mineral surfaces, the step-wave model they employed provides a useful analogy for understanding how microscale surface heterogeneity—such as high kurtosis and valley-rich profiles—can influence dissolution rates in pharmaceutical solids. In the present case, the localized sharp features and negative skewness in the 2 % formulation may act similarly to reactive step edges, facilitating sustained medium penetration and controlled release dynamics. These findings underscore the importance of surfactant content and microstructural characteristics in modulating dissolution kinetics, particularly for poorly soluble APIs.

### 4.7. FTIR spectroscopy

The FTIR analysis provides valuable insight into the compatibility of furosemide with the CuraBlend® excipient matrix and the stability of the drug within the extruded gel tablets. The preservation of the key functional group absorption bands of furosemide in all tablet formulations, including those stored for up to three months, indicates that the drug remains chemically intact and is not subject to major degradation or strong chemical interactionsunder the conditions studied.

The observed reduction in peak intensity and broadening of furosemide bands in the tablet formulations are expected outcomes of the dispersion of the drug within the excipient matrix and the overlapping of excipient absorption bands, particularly from cocoa butter and xylitol.

However, these spectral variations—especially the changes in intensity and shape of the major peaks—may also reflect weak molecular interactions such as hydrogen bonding or matrix entrapment effects. Although no new peaks or substantial shifts were observed, the data suggest the possibility of non-covalent interactions or physical changes related to drug dispersion in the semi-solid matrix. These effects do not imply chemical incompatibility but highlight the importance of considering formulation-level interactions in the interpretation of FTIR data.

The consistency of the FTIR spectra across different formulations and time points further supports the physical and chemical stability of furosemide in the presence of varying concentrations of polysorbate 80. The lack of time-dependent spectral changes, even after three months of storage, suggests that the formulation is robust and capable of maintaining drug integrity over time. Nevertheless, the subtle spectral changes observed should not be dismissed entirely, as they may indicate dynamic interactions within the matrix that could influence drug release or microstructure.This finding is also consistent with the XRD results, which confirm preservation of the primary crystalline features of furosemide while showing minor matrix-related variations.

Overall, the FTIR evaluation confirms that the CuraBlend®-based extruded gel tablet system provides a generally compatible and stableenvironment for furosemide, with no evidence of major degradation or strong chemical interactions. However, the possibility of weak interactions or matrix effects should be acknowledged. These results support the suitability of the selected excipient combination for the development of stable furosemide oral dosage forms and provide a solid foundation for further studies on the performance and shelf-life of the final product.

### 4.8. X-ray powder diffraction

The preservation of characteristic furosemide diffraction peaks across all time points in the 2.6 % polysorbate formulation (Fig. 8) provides evidence for the general physical stability of the drug within the CuraBlend® matrix. While peak intensities are expectedly reduced compared to the pure crystalline powder due to dilution effects, the persistence of these peaks indicates that furosemide remains predominantly in its original crystalline form throughout storage. However, minor variations in peak intensity and broadening suggest that weak molecular interactions or structural dispersion within the matrix cannot be fully excluded. This stability is particularly significant considering the complex excipient environment and potential for drug-excipient interactions in semi-solid extruded formulations. While no major polymorphic transitions or complete amorphization were observed, the subtle spectral changes noted in the XRD patterns over 1.5 years suggest that the formulation design effectively minimizes but may not entirely eliminate matrix-related influences on drug crystallinity.

The data presented in Fig. 9 suggest that while drug loading influences the visibility of furosemide peaks, variations in polysorbate concentration did not have a notable impact on the drug's crystalline structure. The reduced peak definition observed in some formulations—particularly at lower concentrations—may be attributed to the amorphous background of the CuraBlend matrix, which can obscure diffraction signals. Additionally, time-dependent changes such as xylitol crystallization and cocoa butter phase transitions may contribute to the observed patterns. These effects highlight the challenge of interpreting crystalline signals in multi-component systems, where overlapping halos and excipient transitions can mask or modify drug-related peaks.

Taken together, these findings suggest that although the drug's main crystalline features are retained, weak interactions or partial physical integration into the matrix may affect the visibility and shape of specific peaks. This underscores the importance of considering matrix effects and storage conditions during formulation development.

The observed temporal changes in the excipient-related regions of the diffractograms likely reflect the natural reorganization of the semi-crystalline excipient matrix over time. The cocoa butter component of the CuraBlend® base is known to undergo polymorphic transitions and gradual crystallization during storage, which explains some of the observed changes in the medium 2θ region. Importantly, these excipient-related transformations do not appear to significantly disrupt the drug's crystalline structure, as evidenced by the consistent furosemide peak pattern throughout storage. Nonetheless, these observations suggest a dynamic system in which excipient reorganization may influence peak profiles, even if the core crystal form of furosemide is retained. Overall, the XRPD results support the physical stability of furosemide in the formulation but also point to subtle, possibly reversible interactions or dispersion effects. These matrix-related influences, although not chemically transformative, are important to consider when evaluating the robustness and long-term behavior of semi-solid oral dosage forms.

### 4.9. Stability over six months

Stability studies are essential to ascertain the shelf-life and efficacy of pharmaceutical products. Throughout our six-month study, both 1 % and 2 % furosemide gel-based tablets maintained their physical appearance and pH within specified limits. The pH values of both formulations remained stable throughout the six-month study period, ranging between 4.6 and 5.0. Maintaining pH within this range is essential for the stability and solubility of furosemide. Assay values remained within the acceptable range, with less than a 5 % decrease from initial values, indicating chemical stability. Microbiological assessments confirmed the absence of contaminants, ensuring product safety. These results are in line with the requirements outlined in the Ph. Eur. for non-sterile pharmaceutical products and underscore the effectiveness of the manufacturing and packaging processes in preventing microbial contamination.

Building on this technological shift, the current study explores the

use of SSE 3D printing as part of an automated CSS for producing low-dose, immediate-release furosemide tablets tailored to pediatric use. This approach incorporates NIR spectroscopy with chemometric modelling to assess BU during the mixing stage, representing a novel, non-destructive alternative to conventional wet chemistry techniques. Two sampling strategies were employed to generate robust calibration models that account for variability in formulation and process conditions, enabling precise real-time monitoring. Furthermore, the compounding process included live mass uniformity assessments, syringe content homogeneity checks, and content uniformity testing across different levels of the filled syringe to address in-process variability, including heating lag and extrusion dynamics. Final product testing adhered to Ph. Eur. standards, including disintegration, dissolution, and dose uniformity. Additionally, a six-month stability study evaluated both physicochemical attributes and microbiological integrity.

By combining precision manufacturing, real-time analytics, and regulatory-compliant quality control, this study provides a scalable and clinically applicable platform for producing personalized furosemide tablets. It is, to the best of our knowledge, the first to offer an end-to-end, in-process and post-process quality assurance model for SSE-printed pediatric formulations, addressing longstanding gaps in non-sterile compounding automation and setting a new standard for individualized pediatric therapeutics.

## 5. Conclusion

The comprehensive evaluation of 3D-printed gel-based furosemide tablets demonstrates that the formulations meet key quality attributes, including BU, disintegration time, pH stability, microbiological quality, and syringe homogeneity. The use of NIR spectroscopy for in-process control offers a robust method for real-time monitoring, enhancing the efficiency and reliability of the manufacturing process. These findings support the potential of SSE 3D printing technology in producing high-quality, personalized immediate-release tablets.

## Funding

All research infrastructure and materials utilized in this PhD project were generously provided by CurifyLabs. The study has been made possible by funding from the European Innovation Council, EIC (EIC Accelerator grant for the project PMed - Enabling patient specific medicines using 3D printing in hospitals and pharmacies).

## CRediT authorship contribution statement

**Farnaz Shokraneh:** Writing – original draft, Visualization, Validation, Methodology, Investigation, Formal analysis, Data curation, Conceptualization. **Anne M. Filppula:** Writing – review & editing, Supervision, Conceptualization. **Aleksi Tornio:** Writing – review & editing, Supervision. **Jaan Aruväli:** Writing – review & editing, Methodology. **Urve Paaver:** Writing – review & editing, Methodology. **Ivan Kassamakov:** Writing – review & editing, Methodology. **Niklas Sandler Topelius:** Writing – review & editing, Supervision, Methodology, Funding acquisition, Conceptualization.

## Declaration of competing interest

The authors affirm that this research was carried out independently of any commercial or financial interests that might be seen as potential conflicts of interest. CurifyLabs supplied the materials and equipment used in the study. Furthermore, F.S. and N.S.T., who are employed by CurifyLabs, were involved in test planning and data analysis of the research.

## Acknowledgements

We would like to express our heartfelt thanks Mahsa Bahman, Sari Airaksinen, Julius Lahtinen Niko Hassinen and Laura Mantila from the CurifyLabs Pharmaceutical and Analytical R&D team for their invaluable support in carrying out and supporting out these studies.

## Data availability

Data will be made available on request.

## References

Aceves, J.M., Cruz, R., Hernandez, E., 2000. Preparation and characterization of Furosemide-Eudragit controlled release systems. Int. J. Pharm. 195, 45–53. https://doi.org/10.1016/S0378-5173(99)00303-8.

Adrjanowicz, K., Kaminski, K., Grzybowska, K., Hawelek, L., Paluch, M., Gruszka, I., Zakowiecki, D., Sawicki, W., Lepek, P., Kamysz, W., Guzik, L., 2011. Effect of cryogrinding on chemical stability of the sparingly water-soluble drug furosemide. Pharm. Res. 28, 3220–3236. https://doi.org/10.1007/s11095-011-0496-4.

Alhnan, M.A., Okwuosa, T.C., Sadia, M., Wan, K.W., Ahmed, W., Arafat, B., 2016. Emergence of 3D printed dosage forms: opportunities and challenges. Pharm. Res. 33, 1817–1832. https://doi.org/10.1007/s11095-016-1933-1.

Awad, A., Trenfield, S.J., Goyanes, A., Gaisford, S., Basit, A.W., 2018. Reshaping drug development using 3D printing. Drug Discov. Today 23, 1547–1555. https://doi.org/10.1016/j.drudis.2018.05.025.

Baratieri, S.C., Barbosa, J.M., Freitas, M.P., Martins, J.A., 2006. Multivariate analysis of nystatin and metronidazole in a semi-solid matrix by means of diffuse reflectance NIR spectroscopy and PLS regression. J. Pharm. Biomed. Anal. 40, 51–55. https://doi.org/10.1016/j.jpba.2005.05.025.

Blanco, M., Alcalá, M., 2006. Content uniformity and tablet hardness testing of intact pharmaceutical tablets by near infrared spectroscopy. Anal. Chim. Acta 557, 353–359. https://doi.org/10.1016/j.aca.2005.09.070.

Blanco, M., Castillo, M., Peinado, A., Beneyto, R., 2007. Determination of low analyte concentrations by near-infrared spectroscopy: effect of spectral pretreatments and estimation of multivariate detection limits. Anal. Chim. Acta 581, 318–323. https://doi.org/10.1016/j.aca.2006.08.018.

Blanco, M., Villarroya, I., 2002. NIR spectroscopy: a rapid-response analytical tool. TrAC Trends Anal. Chem. 21, 240–250. https://doi.org/10.1016/S0165-9936(02)00404-1.

Bolukbasi, O., Yilmaz, A., 2012. X-ray structure analysis and vibrational spectra of Furosemide. Vib. Spectrosc. 62, 42–49. https://doi.org/10.1016/j.vibspec.2012.06.002.

Bresson, S., Lecuelle, A., Bougrioua, F., El Hadri, M., Baeten, V., Courty, M., Pilard, S., Rigaud, S., Faivre, V., 2021. Comparative structural and vibrational investigations between cocoa butter (CB) and cocoa butter equivalent (CBE) by ESI/MALDI-HRMS, XRD, DSC, MIR and raman spectroscopy. Food Chem. 363, 130319. https://doi.org/10.1016/j.foodchem.2021.130319.

Colella, M.F., Marino, N., Oliviero Rossi, C., Seta, L., Caputo, P., De Luca, G., 2023. Triacylglycerol composition and chemical-physical properties of cocoa butter and its derivatives: NMR, DSC, X-ray, rheological investigation. Int. J. Mol. Sci. 24, 2090. https://doi.org/10.3390/ijms24032090.

Coupland, J.M., Lobera, J., 2010. Measurement of steep surfaces using white light interferometry. Strain 46, 69–78. https://doi.org/10.1111/j.1475-1305.2008.00595.x.

De Beer, T., Burggraeve, A., Fonteyne, M., Saerens, L., Remon, J.P., Vervaet, C., 2011. Near infrared and raman spectroscopy for the in-process monitoring of pharmaceutical production processes. Int. J. Pharm. 417, 32–47. https://doi.org/10.1016/j.ijpharm.2010.12.012.

De Bleye, C., Chavez, P.F., Mantanus, J., Marini, R., Hubert, Ph., Rozet, E., Ziemons, E., 2012. Critical review of near-infrared spectroscopic methods validations in pharmaceutical applications. J. Pharm. Biomed. Anal. 69, 125–132. https://doi.org/10.1016/j.jpba.2012.02.003.

Development and Submission of Near Infrared Analytical Procedures, 2021.

Eileen Kairuz, T., Gargiulo, D., Bunt, C., Garg, S., 2007. Quality, safety and efficacy in the 'Off-label' use of medicines. Curr. Drug Saf. 2, 89–95. https://doi.org/10.2174/157488607779315471.

Foo, W.C., Widjaja, E., Khong, Y.M., Gokhale, R., Chan, S.Y., 2018. Application of miniaturized near-infrared spectroscopy for quality control of extemporaneous orodispersible films. J. Pharm. Biomed. Anal. 150, 191–198. https://doi.org/10.1016/j.jpba.2017.11.068.

Gallignani, M., Rondón, R.A., Ovalles, J.F., Brunetto, M.R., 2014. Transmission FTIR derivative spectroscopy for estimation of furosemide in raw material and tablet dosage form. Acta Pharm. Sin. B 4, 376–383. https://doi.org/10.1016/j.apsb.2014.06.013.

Genina, N., Fors, D., Vakili, H., Ihalainen, P., Pohjala, L., Ehlers, H., Kassamakov, I., Haeggström, E., Vuorela, P., Peltonen, J., Sandler, N., 2012. Tailoring controlled-release oral dosage forms by combining inkjet and flexographic printing techniques. Eur. J. Pharm. Sci. 47, 615–623. https://doi.org/10.1016/j.ejps.2012.07.020.

Goyanes, A., Scarpa, M., Kamlow, M., Gaisford, S., Basit, A.W., Orlu, M., 2017. Patient acceptability of 3D printed medicines. Int. J. Pharm. 530, 71–78. https://doi.org/10.1016/j.ijpharm.2017.07.064.

Granero, G.E., Longhi, M.R., Mora, M.J., Junginger, H.E., Midha, K.K., Shah, V.P., Stavchansky, S., Dressman, J.B., Barends, D.M., 2010. Biowaiver monographs for immediate release solid oral dosage forms: furosemide. J. Pharm. Sci. 99, 2544–2556. https://doi.org/10.1002/jps.22030.

Gudeman, J., Jozwiakowski, M., Chollet, J., Randell, M., 2013. Potential risks of pharmacy compounding. Drugs RD 13, 1–8. https://doi.org/10.1007/s40268-013-0005-9.

ICH Q2(R2): Validation of analytical procedures, 2003.

Johannesson, J., Wu, M., Johansson, M., Bergström, C.A.S., 2023. Quality attributes for printable emulsion gels and 3D-printed tablets: towards production of personalized dosage forms. Int. J. Pharm. 646, 123413. https://doi.org/10.1016/j.ijpharm.2023.123413.

Kassamakov, I.Vl., Seppänen, H.O., Oinonen, M.J., Hæggström, E.O., Österberg, J.M., Aaltonen, J.P., Saarikko, H., Radivojevic, Z.P., 2007. Scanning white light interferometry in quality control of single-point tape automated bonding. Microelectron. Eng. 84, 114–123. https://doi.org/10.1016/j.mee.2006.08.013.

Khaled, S.A., Burley, J.C., Alexander, M.R., Roberts, C.J., 2014. Desktop 3D printing of controlled release pharmaceutical bilayer tablets. Int. J. Pharm. 461, 105–111. https://doi.org/10.1016/j.ijpharm.2013.11.021.

Khaled, S.A., Burley, J.C., Alexander, M.R., Yang, J., Roberts, C.J., 2015. 3D printing of five-in-one dose combination polypill with defined immediate and sustained release profiles. J. Control. Release 217, 308–314. https://doi.org/10.1016/j.jconrel.2015.09.028.

Lafeber, I., Tichem, J.M., Ouwerkerk, N., Van Unen, A.D., Van Uitert, J.J.D., Bijleveld-Olierook, H.C.M., Kweekel, D.M., Zaal, W.M., Le Brun, P.P.H., Guchelaar, H.J., Schimmel, K.J.M., 2021. 3D printed furosemide and sildenafil tablets: innovative production and quality control. Int. J. Pharm. 603, 120694. https://doi.org/10.1016/j.ijpharm.2021.120694.

Mantanus, J., Ziémons, E., Lebrun, P., Rozet, E., Klinkenberg, R., Streel, B., Evrard, B., Hubert, P., 2009. Moisture content determination of pharmaceutical pellets by near infrared spectroscopy: method development and validation. Anal. Chim. Acta 642, 186–192. https://doi.org/10.1016/j.aca.2008.12.031.

Markl, D., Zeitler, J.A., 2017. A review of disintegration mechanisms and measurement techniques. Pharm. Res. 34, 890–917. https://doi.org/10.1007/s11095-017-2129-z.

Matawo, N., Adeleke, O.A., Wesley-Smith, J., 2020. Optimal design, characterization and preliminary safety evaluation of an edible orodispersible formulation for pediatric tuberculosis pharmacotherapy. Int. J. Mol. Sci. 21, 5714. https://doi.org/10.3390/ijms21165714.

Mullarkey, T., 2009. Pharmacy compounding of high-risk level products and patient safety. Am. J. Health Syst. Pharm. 66, S4–S13. https://doi.org/10.2146/ajhp0108b.

Norman, J., Madurawe, R.D., Moore, C.M.V., Khan, M.A., Khairuzzaman, A., 2017. A new chapter in pharmaceutical manufacturing: 3D-printed drug products. Adv. Drug Deliv. Rev. 108, 39–50. https://doi.org/10.1016/j.addr.2016.03.001.

O Mahony, C., Hill, M., Brunet, M., Duane, R., Mathewson, A., 2003. Characterization of micromechanical structures using white-light interferometry. Meas. Sci. Technol. 14, 1807–1814. https://doi.org/10.1088/0957-0233/14/10/310.

Paaver, U., Heinämäki, J., Kassamakov, I., Hæggström, E., Ylitalo, T., Nolvi, A., Kozlova, J., Laidmäe, I., Kogermann, K., Veski, P., 2014. Nanometer depth resolution in 3D topographic analysis of drug-loaded nanofibrous mats without sample preparation. Int. J. Pharm. 462, 29–37. https://doi.org/10.1016/j.ijpharm.2013.12.041.

Paris, I., Janoly-Dumenil, A., Paci, A., Mercier, L., Bourget, P., Brion, F., Chaminade, P., Rieutord, A., 2006. Near infrared spectroscopy and process analytical technology to master the process of busulfan paediatric capsules in a university hospital. J. Pharm. Biomed. Anal. 41, 1171–1178. https://doi.org/10.1016/j.jpba.2006.02.049.

Pasquini, C., 2018. Near infrared spectroscopy: a mature analytical technique with new perspectives–a review. Anal. Chim. Acta 1026, 8–36. https://doi.org/10.1016/j.aca.2018.04.004.

Prandota, J., 2001. Clinical pharmacology of Furosemide in children: a supplement. Am. J. Ther. 8, 275–289. https://doi.org/10.1097/00045391-200107000-00010.

Rinke, M.L., Shore, A.D., Morlock, L., Hicks, R.W., Miller, M.R., 2007. Characteristics of pediatric chemotherapy medication errors in a national error reporting database. Cancer 110, 186–195. https://doi.org/10.1002/cncr.22742.

Rinnan, Å., Berg, F.V.D., Engelsen, S.B., 2009. Review of the most common pre-processing techniques for near-infrared spectra. TrAC Trends Anal. Chem. 28, 1201–1222. https://doi.org/10.1016/j.trac.2009.07.007.

Roggo, Y., Chalus, P., Maurer, L., Lema-Martinez, C., Edmond, A., Jent, N., 2007. A review of near infrared spectroscopy and chemometrics in pharmaceutical technologies. J. Pharm. Biomed. Anal. 44, 683–700. https://doi.org/10.1016/j.jpba.2007.03.023.

Roostar, K., Meos, A., Laidmäe, I., Aruväli, J., Räikkönen, H., Peltonen, L., Airaksinen, S., Topelius, N.S., Heinämäki, J., Paaver, U., 2025. Towards a customized oral drug therapy for pediatric applications: chewable propranolol gel tablets printed by an automated extrusion-based material deposition method. Pharmaceutics 17, 881. https://doi.org/10.3390/pharmaceutics17070881.

Sandler, N., Kassamakov, I., Ehlers, H., Genina, N., Ylitalo, T., Haeggstrom, E., 2014. Rapid interferometric imaging of printed drug laden multilayer structures. Sci. Rep. 4, 4020. https://doi.org/10.1038/srep04020.

Sandler, N., Preis, M., 2016. Printed drug-delivery systems for improved patient treatment. Trends Pharmacol. Sci. 37, 1070–1080. https://doi.org/10.1016/j.tips.2016.10.002.

Sandler Topelius, N., Shokraneh, F., Bahman, M., Lahtinen, J., Hassinen, N., Airaksinen, S., Verma, S., Hrizanovska, L., Lass, J., Paaver, U., Tähnas, J., Kern, C., Lagarce, F., Fenske, D., Malik, J., Scherliess, H., Cruz, S.P., Paulsson, M., Dekker, J., Kammonen, K., Rautamo, M., Lück, H., Pierrot, A., Stareprawo, S., Tubic-Grozdanis, M., Zibolka, S., Lösch, U., Jeske, M., Griesser, U., Hummer, K., Thalmeier, A., Harjans, A., Kruse, A., Heimke-Brinck, R., Khoukh, K., Bruno, F., 2024. Automated non-sterile pharmacy compounding: a multi-site study in European Hospital and Community pharmacies with pediatric immediate release propranolol hydrochloride tablets. Pharmaceutics 16, 678. https://doi.org/10.3390/pharmaceutics16050678.

Sarraguça, M.C., Lopes, J.A., 2009. Quality control of pharmaceuticals with NIR: from lab to process line. Vib. Spectrosc. 49, 204–210. https://doi.org/10.1016/j.vibspec.2008.07.013.

Shokraneh, F., Filppula, A.M., Tornio, A., Aruväli, J., Paaver, U., Topelius, N.S., 2025. Automated extrusion-based dispensing: personalized dosing and quality control of clopidogrel tablets for pediatric care. Eur. J. Pharm. Sci. 204, 106967. https://doi.org/10.1016/j.ejps.2024.106967.

Simpson, M.B., 2005. Near-infrared spectroscopy for process analytical chemistry: theory, technology and implementation. In: Bakeev, K.A. (Ed.), Process Analytical Technology. Wiley, pp. 39–90. https://doi.org/10.1002/9780470988459.ch3.

Soriano, M.L., Zougagh, M., Ríos, Á., Valcárcel, M., 2019. Analytical reliability of simple, rapid, minuturizated, direct analytical processes: a call to arms. TrAC Trends Anal. Chem. 114, 98–107. https://doi.org/10.1016/j.trac.2019.03.005.

Trenfield, S.J., Awad, A., Goyanes, A., Gaisford, S., Basit, A.W., 2018. 3D printing pharmaceuticals: drug development to frontline care. Trends Pharmacol. Sci. 39, 440–451. https://doi.org/10.1016/j.tips.2018.02.006.

van der Vorst, M.M.J., Kist, J.E., van der Heijden, A.J., Burggraaf, J., 2006. Diuretics in pediatrics: current knowledge and future prospects. Paediatr. Drugs 8, 245–264. https://doi.org/10.2165/00148581-200608040-00004.

Van Der Zanden, T.M., Mooij, M.G., Vet, N.J., Neubert, A., Rascher, W., Lagler, F.B., Male, C., Grytli, H., Halvorsen, T., De Hoog, M., De Wildt, S.N., 2021. Benefit-risk assessment of off-label drug use in children: the Bravo framework. Clin. Pharmacol. Ther. 110, 952–965. https://doi.org/10.1002/cpt.2336.

Van Riet-Nales, D.A., De Jager, K.E., Schobben, A.F.A.M., Egberts, T.C.G., Rademaker, C. M.A., 2011. The availability and age-appropriateness of medicines authorized for children in the Netherlands. Br. J. Clin. Pharmacol. 72, 465–473. https://doi.org/10.1111/j.1365-2125.2011.03982.x.

Wang, X., Fu, Q., Sheng, J., Yang, X., Jia, J., Du, W., 2010. Construction of a universal quantitative model for ibuprofen sustained-release capsules from different manufacturers using near-infrared diffuse reflection spectroscopy. Vib. Spectrosc. 53, 214–217. https://doi.org/10.1016/j.vibspec.2010.03.002.

Whitelaw, A., Brion, L.P., Kennedy, C.R., Odd, D., 2001. Diuretic therapy for newborn infants with posthemorrhagic ventricular dilatation. Cochrane Database Syst. Rev. 2010. https://doi.org/10.1002/14651858.CD002270.

Workman Jr., Jerry, Weyer, L., 2007. Practical Guide to Interpretive Near-Infrared Spectroscopy. CRC Press. https://doi.org/10.1201/9781420018318, 0 ed.

Yang, T.L., Szewc, J., Zhong, L., Leonova, A., Giebułtowicz, J., Habashy, R., Isreb, A., Alhnan, M.A., 2023. The use of near-infrared as process analytical technology (PAT) during 3D printing tablets at the point-of-care. Int. J. Pharm. 642, 123073. https://doi.org/10.1016/j.ijpharm.2023.123073.

Yu, L., Ding, J., 2008. Injectable hydrogels as unique biomedical materials. Chem. Soc. Rev. 37, 1473. https://doi.org/10.1039/b713009k.